VILNIUS UNIVERSITY
CENTER FOR PHYSICAL SCIENCES AND TECHNOLOGY
INSTITUTE OF PHYSICS

Mindaugas Gedvilas

SELF-ORGANIZATION IN THIN METAL FILMS UNDER LASER IRRADIATION

Doctoral dissertation
Technological Sciences, Material Engineering (08T)
Laser Technology (T165)

Vilnius, 2011

The research was performed in the Institute of Physics of Center for Physical Sciences and Technology in 2006-2011.

Scientific supervisor:

Dr. Gediminas Račiukaitis (Institute of Physics of Center for Physical Sciences and Technology, technological sciences, material engineering - 08T, laser technology - T165).

VILNIAUS UNIVERSITETAS
FIZINIŲ IR TECHNOLOGIJOS MOKSLŲ CENTRO
FIZIKOS INSTITUTAS

Mindaugas Gedvilas

PLONŲ METALŲ SLUOKSNIŲ SAVITVARKOS LAZERIO SPINDULIUOTĖS POVEIKYJE TYRIMAS IR MODELIAVIMAS

Daktaro disertacija
Technologijos mokslai, Medžiagų inžinerija (08T)
Lazerinė technologija (T165)

Vilnius, 2011

Disertacija rengta 2006-2011 metais Fizinių ir Technologijos Mokslų Centro Fizikos institute.

Mokslinis vadovas:

Dr. Gediminas Račiukaitis (Fizinių ir technologijos mokslų centro Fizikos institutas, technologijos mokslai, medžiagų inžinerija - 08T, lazerinė technologija - T165).

CONTENTS

ACKNOWLEDGMENTS

The work was supported by the Lithuanian State Science and Studies Foundation under projects No B21/2006 and B31/2008.

I am very grateful to my scientific supervisor Dr. G. Račiukaitis for endless patience and huge support.

Thanks to Dr. M. Brikas for introduction to my supervisor Dr. G. Račiukaitis.

Thanks to my colleague Dr. K. Regelskis for valuable discussions.

Thanks to my colleagues B. Voisiat, E. Stankevičius, P. Gečys, R. Trusovas, G. Darčianovas, V. Kučikas, S. Grubinskas, S. Indrišiūnas and Dr. M. Maciulevičius for friendly atmosphere in the laboratory.

I express my thanks to Dr. A. Selskis from the Institute of Chemistry of Center for Physical Sciences and Technology, Vilnius for technical assistance and Prof. E. Ohmura from Osaka University for fruitful discussions.

I would also like to thank my family and friends for support during never-ending studies.

LIST OF ABBREVIATIONS

List of acronyms

μm	Micrometer (10^{-6} m)
3D	Three dimensional
AFM	Atomic force microscopy
CW	Continuous wave
fs	Femtosecond (10^{-15} s)
HAZ	Heat affected zone
IR	Infrared
ISI	Institute of Scientific Information
LIPSS	Laser induced periodical surface structures
Nd:YAG	Neodymium-doped yttrium aluminum garnet ($Nd:Y_3Al_5O_{12}$)
nm	Nanometer (10^{-9} m)
ns	Nanosecond (10^{-9} s)
PC	Pockels cell
ps	Picosecond (10^{-12} s)
SEM	Scanning electron microscope
TTM	Two temperature model
UV	Ultraviolet
WoS	Web of Science

List of symbols

A_λ	Absorptivity, [-]
A_H	Hamaker constant, [J]
C_p	Specific heat capacity, [$J \cdot kg^{-1}$]
d	Ablation depth per pulse (ablation rate), [$m \cdot pulse^{-1}$]
D	Diameter of ablated (modified) area, [m]
D_{haz}	Depth of the Heat affected zone, [m]
E	Young's modulus, [Pa]

E_p	Laser pulse energy, [J]
f	Focal length, [m]
F	Laser fluence, [$J \cdot m^{-2}$]
F_0	Peak laser fluence, [$J \cdot m^{-2}$]
f_{Rep}	Pulse repetition rate, [Hz]
h	Film thickness, [m]
I	Laser intensity, [$W \cdot m^{-2}$]
k	Extinction coefficient (imaginary part of refractive index), [-]
L_m	Heat of fusion, [$J \cdot kg^{-1}$]
L_v	Heat of vaporization, [$J \cdot kg^{-1}$]
m	Diffraction order, [Integer]
M	Standard atomic weight, [$kg \cdot mol^{-1}$]
M^2	Beam quality factor, [-]
Ma	Marangoni number, [-]
$\tilde{n}$	Refractive index (complex number), [-]
N	Number of pulses per spot, [-]
n	Refractive index (real part of refractive index), [-]
p	Pressure, [Pa]
R_λ	Reflectivity, [-]
R^*	Gas constant, [$J \cdot mol^{-1} \cdot K^{-1}$]
T	Temperature, [K]
t	Time, [s]
T_m	Melting point, [K]
T_v	Boiling point, [K]
T_λ	Transmittance, [-]
u	Marangoni speed, [$m \cdot s^{-1}$]
V	Atomic or molar volume, [$m^3 \cdot mol^{-1}$]
v	Scanning speed, [$m \cdot s^{-1}$]
w_0	Gaussian beam radius, [m]
x, y, z	Spatial coordinates, [m]

List of Greek symbols

α	Absorption coefficient, [m^{-1}]
α_{diff}	Thermal diffusivity, [$s\cdot m^{-2}$]
α_{eff}	Effective absorption coefficient, [m^{-1}]
β	Thermal expansion coefficient, [K^{-1}]
γ	Surface tension of liquid, [$N\cdot m^{-1}$]
ΔT	Temperature difference, [K]
Δx	Shift between pulses, [m]
ε	Strain, [-]
η	Dynamic viscosity, [$N\cdot s\cdot m^{-2}$]
κ	Thermal conductivity, [$W\cdot K^{-1}\cdot m^{-1}$]
Λ	Ripple period, [m]
λ	Wavelength of laser radiation, [m]
ν	Poisson ratio, [-]
ρ	Density, [$kg\cdot m^{-3}$]
σ	Stress, [Pa]
τ	Shear stress, [Pa]
τ_p	Pulse duration, [s]
φ	Diffraction angle, [rad]

1 INTRODUCTION

Metal films on glass are widely used in industry and science and cover diverse applications. The chromium film on glass is an important material in the photo mask production for lithography [1-3], as well as in production of diffraction gratings [4], and linear optical encoders for metrology [5, 6]. Aluminum and silver are used as mirrors [7], and gold films are widely applied in bio-medicine as a substrate for bio-chip production [8].

Lasers are frequently applied for patterning the metal film instead of the wet chemical or plasma etching [9]. When performing micromachining using lasers, multiple bursts of lower power irradiation are employed to minimize heating. However, ripples, or laser-induced periodic surface structures, are observed at intensities near the ablation threshold [10]. Transformation of the metal film structure under laser beam irradiation is to some extent an undesirable effect but at same time it is a promising method for micro and nano-structuring of the functional surfaces [11]. Laser-direct writing using front-side and rear-side ablation with a femtosecond laser was applied in the photomask production [12]. During the rare-side machining the film was removed by explosion because heating was localized at the inner interface between the film and the substrate. The sub-diffraction limit precision was achieved with the femtosecond laser pulses and was applied for the mask repair [13, 14].

In our industrial project in collaboration with “Precizika Metrology” laser technology for production of linear optical encoders for metrology was developed. The beam of a nanosecond laser tightly focused to a line was applied for the back-side ablation of the chromium thin film on a glass substrate. The stripe of the film ablated with a single laser pulse had sharp edges on both sides and ridges of the melted metal around it. Optical linear encoders with the period of several micrometers were produced. When trying to pass on to smaller periods unusual behavior of chromium film on glass was observed during ablation experiments with the partially overlapping pulses

[15]. In a certain range of laser fluences and pulse overlap, the remaining metal tended to self-organize into ripples, which were orientated perpendicularly to the laser spot extent. Origin of the ripples was completely different from that observed near the ablation threshold [16]. Set of experiments and modeling procedures were implemented in order to understand physical processes causing self-organization of the metal film into regular structures. Depending on the process parameters, the ripple formation was regular.

In this thesis, the experimental and theoretical results of new self-organization of the thin metal film on the glass substrate by using IR nanosecond laser radiation with a specially shaped beam are presented. The method for formation of regular ripples and results on investigation of diffractive properties of the self-organized gratings are presented.

1.1 THE AIM OF THE RESEARCH

1. To find out mechanisms of the ripple initiation and formation in the chromium thin film on the glass substrate.
2. To learn how to control the ripple formation and to apply it for fabrication of diffraction gratings.

1.2 PRACTICAL VALUE AND NOVELTY

1.2.1 The novelty of the thesis

1. A novel phenomenon of self-organization in the chromium thin film on the glass substrate initiated by nanosecond-laser radiation has been observed and its origin has been investigated. Regular ripples can be formed in a certain region of laser processing parameters, mainly, the peak laser fluence and the shift between laser pulses.
2. A model of the ripple formation has been developed. Plateau-Rayleigh instability in a cylindrical ridge of the molten metal on a rim of the laser

ablated area was found to be an initiator at the beginning of the ripple formation. Marangoni (thermo-capillarity) flow stabilized the process and led to a steady and regular growth of ripples along the scanning direction by irradiation with partially overlapping laser pulses.

3. Experiments with different metals proved that the ridge formation during laser ablation was essential for initiation of the ripple formation. The ridge formation depends of the adhesion of the metal film with the glass substrate as well as on thermo-physical parameters of the metal which determine the Marangoni force.

1.2.2 The practical value of the thesis

1. The new method of diffraction grating fabrication in thin metal films on glass has been developed and verified. Period of the grating can be controlled in the range of 2.5 - 4.0 μm for the 100 nm thick chromium film on the glass substrate.

2. As the self-organization in metal films under laser irradiation is an unwanted side effect in production of photomask for lithography and linear optical encoders for metrology, understanding of the processes, which are responsible for ripple formation in the thin metal film, can be used to avoid or reduce its effect on the precision and quality of laser structuring for the applications.

1.3 STATEMENTS TO BE DEFENDED

1. Plateau-Rayleigh instability during formation of a cylindrical ridge of molten metal on a rim of the laser ablated area is responsible for initiation of the ripple formation in thin chromium film on the glass substrate.

2. The steady state of the ripple formation in the thin chromium film during laser irradiation with the sequence of partially overlapping laser pulses is caused by the Marangoni convection effect. The thermal gradient of the surface

tension pushes molten chromium from hotter to colder areas stabilizing the process of the regular ripples formation along the scanning direction.

3. Metal adhesion to the glass substrate is essential for the ridge formation during laser ablation and the ridge is necessary to trigger the Plateau-Rayleigh instability and the ripple formation.

4. Ripple formation by self-organization in the laser-irradiated chromium thin film is a promising technique for manufacturing of diffraction gratings.

1.4 APPROBATION

Results of the research, presented in the thesis, were published in 5 scientific papers [A1-A5] and together with coauthors the results were presented in 9 contributions to conferences [C1-C9]. In total, my publication list includes 20 scientific papers and 38 presentations at the conferences.

1.4.1 Scientific papers

Publications related to the topic of the thesis (ISI WoS – with Conference Proceedings)

[A1] M. Gedvilas, B. Voisiat, G. Račiukaitis and K. Regelskis, Self-organization in thin metal films after irradiation with nanosecond laser pulses. *Appl. Surf. Sci.* **255**, 9826-9829 (2009).

[A2] M. Gedvilas, G. Račiukaitis, K. Regelskis and P. Gečys, Formation of gratings by self-organization of chromium thin film on the glass substrate under irradiation with laser pulses. *J. Laser Micro/Nanoeng.* **3**, 58-62 (2008).

[A3] M. Gedvilas, G. Račiukaitis and K. Regelskis, Self-organization in chromium thin film under laser irradiation. *Appl. Phys. A. Mater. Sci. Process.* **93**, 203-208 (2008).

[A4] K. Regelskis, G. Račiukaitis and **M. Gedvilas**, Ripple Formation in Chromium Thin Film during Laser Ablation. *Appl. Surf. Sci.* **253**, 6584-6587 (2007).

Other publications related to the topic of the thesis

[A5] M. Gedvilas, G. Račiukaitis, K. Regelskis and P. Gečys, Fabrication of gratings by self-organization of thin metal film. *Acta Universitatis Lappeenrantaensis* **273**, 482-492 (2007).

Publications not directly related to the thesis (ISI WoS – with Conference Proceedings)

[A6] B. Voisiat, **M. Gedvilas**, S. Indrišiūnas and G. Račiukaitis, Picosecond-laser 4-beam-interference ablation as a flexible tool for thin film microstructuring. *Physics procedia* **12**, 116-124 (2011).

[A7] G. Račiukaitis, E. Stankevičius, P. Gečys, **M. Gedvilas**, C. Bischoff, E. Jäger, U. Umhofer and F. Völklein, Laser processing by using diffractive optical laser beam shaping technique. *J. Laser Micro/Nanoeng.* **6**, 37-43 (2011).

[A8] G. Račiukaitis, P. Gečys, **M. Gedvilas**, K. Regelskis and B. Voisiat, Selective Ablation of Thin Films with Picosecond-Pulsed Lasers for Solar Cells. *AIP Conf. Proc.* **1278**, 800-811 (2010).

[A9] P. Gečys, G. Račiukaitis, M. Ehrhardt, K. Zimmer and **M. Gedvilas**, Ps-laser scribing of CIGS films at different wavelengths. *Appl. Phys. A Mater. Sci. Process.* **101**, 373-378 (2010).

[A10] E. Molotokaitė, **M. Gedvilas**, G. Račiukaitis and V. Girdauskas, Picosecond laser beam interference ablation of thin metal film on glass substrate. *J. Laser Micro/Nanoeng.* **5**, 74-79 (2010).

[A11] P. Gečys, G. Račiukaitis, **M. Gedvilas** and A. Selskis, Laser Structuring of Thin-Film Solar Cells on Polymers. *Eur. Phys. J. Appl. Phys.* **46**, 12508 (2009).

[A12] G. Račiukaitis, M. Brikas, P. Gečys, B. Voisiat and **M. Gedvilas**, Use of High Repetition Rate and High Power Lasers in Microfabrication: How to Keep the Efficiency High?. *J. Laser Micro/Nanoeng.* **4**, 186-191 (2009).

[A13] G. Račiukaitis, M. Brikas, P. Gečys and **M. Gedvilas**, Accumulation effects in laser ablation of metals with high-repetition rate lasers. *Proc. SPIE* **7005**, 70052L (2008).

[A14] G. Račiukaitis, M. Brikas, **M. Gedvilas** and T. Rakickas, Patterning of Indium-Tin Oxide on Glass with Picosecond Lasers. *Appl. Surf. Sci.* **253**, 6570-6574 (2007).

[A15] G. Račiukaitis, M. Brikas, **M. Gedvilas** and G. Darčianovas, Patterning of ITO with Picosecond Lasers. *Proc. SPIE* **6596**, 65960M (2007).

[A16] G. Račiukaitis, M. Brikas, **M. Gedvilas** and G. Darčianovas, Patterning of ITO layer on glass with high repetition rate picosecond lasers. *J. Laser Micro/Nanoeng.* **2**, 1-6 (2007).

[A17] M. Gedvilas and G. Račiukaitis, Investigation of UV picosecond laser ablation of polymers. *Proc. SPIE* **6157**, 61570T (2005).

[A18] O. Scharf, G. Gaigalas, S. Fritzsche, **M. Gedvilas**, E. Gaidamauskas and G. Kiršanskas, Application of the RACAH package for dealing with the expressions from the atomic shell model. *Nucl. Instrum. Methods Phys. Res. B* **235**, 135-139 (2005).

Other publications not directly related to the thesis

[A19] E. Stankevičius, M. Malinauskas, **M. Gedvilas**, B. Voisiat and G. Račiukaitis, Fabrication of Periodic Micro-Structures by Multi-Photon Polymerization Using Femtosecond Laser and Four-Beam Interference. *Matter. Sci. (Medžiagotyra)* **16**, 1392-1320 (2010).

[A20] M. Brikas, G. Račiukaitis and **M. Gedvilas**, Accumulation effects during processing of metals and silicon with repetition-rate lasers. *Acta Universitatis Lappeenrantaensis* **273**, 645-656 (2007).

1.4.2 Conference presentations

Presentations directly related to the topic of the thesis

[C1] V. Kučikas, **M. Gedvilas** and S. Grubinskas, *Modeling of Self-organization in Thin Metal Layers under Laser Irradiation*, 54th Scientific Conference for Students of Physics and Natural Sciences "Open Readings 2011", Vilnius, Lithuania, March 17-19, 2011.

[C2] G. Račiukaitis, **M. Gedvilas**, B. Voisiat, E. Molotokaitė and K. Regelskis, *Transformations in thin metal films induced by laser irradiation*, The Conference "Northern Optics 2009" (NO 2009), Vilnius, Lithuania, August 26-28, 2009.

[C3] M. Gedvilas, G. Račiukaitis, B. Voisiat and K. Regelskis, *Simulation of ripple formation induced by laser irradiation in chromium film on glass substrate*, "38-oji Lietuvos nacionalinė fizikos konferencija", Vilnius, Lithuania, June 8-10, 2009.

[C4] M. Gedvilas, B. Voisiat, G. Račiukaitis and K. Regelskis, *Self-organization in thin metal films after irradiation with nanosecond laser pulses*, "6th International Conference on Photo-Excited Processes and Applications" (6-ICPEPA), Sapporo, Japan, September 9-12, 2008.

[C5] M. Gedvilas, B. Voisiat, K. Regelskis and P. Gečys, *Ripple formation by laser irradiation and FEMLAB simulation*, 1st International School on "Laser-surface interactions for new materials production: tailoring structure and properties", Venice, Italy, July 13-20, 2008.

[C6] M. Gedvilas, G. Račiukaitis and K. Regelskis, *Self-organization in chromium thin film under laser irradiation*, The 9th International "Conference on Laser Ablation" (COLA 2007), Tenerife, Spain, September 24-28, 2007.

[C7] K. Regelskis, **M. Gedvilas**, G. Račiukaitis and P. Gečys, *Fabrication of gratings by self-organization of thin metal film*, "The 11th Nordic Conference in Laser Materials Processing" (11-NOLAMP), Lappeenranta, Finland, August 20-22, 2007.

[C8] M. Gedvilas, K. Regelskis, P. Gečys and G. Račiukaitis, *Formation of gratings by self-organization of chromium thin film under irradiation with laser pulses*, "37-oji Lietuvos nacionalinė fizikos konferencija", Vilnius, Lithuania, June 11-13, 2007.

[C9] M. Gedvilas, G. Račiukaitis, K. Regelskis and P. Gečys, *Formation of gratings by self-organization of chromium thin film on the glass substrate under irradiation with laser pulses*, The International Symposium on "Laser Precision Microfabrication" (LPM 2007), Vienna, Austria, April 24-28, 2007. (Student Poster Award).

Contribution to other presentations at conferences

[C10] B. Voisiat, **M. Gedvilas**, B. Abakevičienė, S. Tamulevičius and G. Račiukaitis, *Micro-channel formation for solid oxide fuel cells using laser beam interference ablation*, The 12th International Symposium on "Laser Precision Microfabrication" (LPM2011), Takamatsu, Kagawa, Japan, June 7-10, 2011.

[C11] M. Maciulevičius, **M. Gedvilas**, B. Abakevičienė, S. Tamulevičius and G. Račiukaitis, *Laser drilling of Ni film on silicon for μ-SOFC*, The 12th International Symposium on "Laser Precision Microfabrication" (LPM2011), Takamatsu, Kagawa, Japan, June 7-10, 2011.

[C12] B. Voisiat, **M. Gedvilas**, S. Indrišiūnas and G. Račiukaitis, *Flexible microstructuring of thin films using multi-beam interference ablation with ultrashort lasers*, The 12th International Symposium on "Laser Precision Microfabrication" (LPM2011), Takamatsu, Kagawa, Japan, June 7-10, 2011.

[C13] G. Račiukaitis, P. Gečys, S. Grubinskas, **M. Gedvilas**, A. Braun and S. Ragnow, *Progress in picosecond-laser scribing for CIGS solar cells*, The 12th International Symposium on "Laser Precision Microfabrication" (LPM2011), Takamatsu, Kagawa, Japan, June 7-10, 2011.

[C14] G. Račiukaitis, P. Gečys, **M. Gedvilas**, K. Regelskis and B. Voisiat, *Selective Ablation of Thin Films with Ultra-Short-Pulse Lasers for Solar Cells and Other Technical Applications*, The International "High Power Laser

Ablation" Conference (HPLA 2010), Santa Fe, New Mexico, USA, April 18-22, 2010.

[C15] P. Gečys, G. Račiukaitis, **M. Gedvilas** and A. Selskis, *Laser structuring of thin-film solar cells on polymers*, "12th Nordic Conference in Laser Processing of Materials" (12-NOLAMP), Copenhagen, Denmark, August 24-26, 2009.

[C16] M. Gedvilas, E. Molotokaitė, G. Račiukaitis and V. Girdauskas, *Picosecond laser beam interference ablation*, "12th Nordic Conference in Laser Processing of Materials" (12-NOLAMP), Copenhagen, Denmark, August 24-26, 2009.

[C17] E. Molotokaitė, **M. Gedvilas**, G. Račiukaitis and V. Girdauskas, *Picosecond laser beam interference ablation of chromium thin film on glass substrate*, The 5th International Congress on "Laser Advanced Materials Processing" (LAMP 2009), Kobe, Japan, June 30 - July 2, 2009.

[C18] M. Gedvilas, G. Račiukaitis and V. Girdauskas, *Structuring of Metal Films by the Laser Beam Interference Ablation*, WLT-Conference "Lasers in Manufacturing" (LIM 2009), Munich, Germany, June 15-18, 2009.

[C19] E. Navickas, S. Tamulevičius, **M. Gedvilas** and G. Račiukaitis, Laser drilling of YSZ – NiO – Ni cermet thin films, "38-oji Lietuvos nacionalinė fizikos konferencija", Vilnius, Lithuania, June 8-10, 2009.

[C20] G. Račiukaitis, M. Brikas, P. Gečys and **M. Gedvilas**, *Laser Structuring of Electro-Conducting Layers for Thin-Film Electronic Devices*, "38-oji Lietuvos nacionalinė fizikos konferencija", Vilnius, Lithuania, June 8-10, 2009.

[C21] E. Molotokaitė, **M. Gedvilas**, B. Voisiat, M. Gabalis and V. Girdauskas, *Picosecond laser beam interference ablation of thin films*, "38-oji Lietuvos nacionalinė fizikos konferencija", Vilnius, Lithuania, June 8-10, 2009.

[C22] G. Račiukaitis, M. Brikas and **M. Gedvilas**, *Efficiency aspects in processing of metals with high-repetition-rate ultra-short-pulse lasers*, "International Congress on Applications of Lasers & Electro-Optics" (ICALEO 2008), Temecula, California, USA, October 20-24, 2008.

[C23] G. Račiukaitis, P. Gečys and **M. Gedvilas**, *Laser structuring of conducting films on transparent substrates for electronics devices*, "International Congress on Applications of Lasers & Electro- Optics" (ICALEO 2008), Temecula, California, USA, October 20-24, 2008.

[C24] P. Gečys, G. Račiukaitis, **M. Gedvilas** and A. Selskis, *Laser Structuring of Thin-Film Solar Cells on Polymers*, "1st International Symposium on Flexible Organic Electronics" (IS-FOE), Halkidiki, Greece, July 10-11, 2008.

[C25] G. Račiukaitis, M. Brikas, P. Gečys, B. Voisiat and **M. Gedvilas**, *Use of High Repetition Rate and High Power Lasers in Microfabrication: How to Keep the Efficiency High?*, 9th International Symposium on "Laser Precision Microfabrication" (LPM 2008), Quebec City, Canada, June 16-20, 2008.

[C26] G. Račiukaitis, M. Brikas, P. Gečys and **M. Gedvilas**, *Accumulation effects in laser ablation of metals with high-repetition rate lasers*, SPIE Conference on "High-Power Laser Ablation" (HPLA 2008), Taos, New Mexico, USA, April 20-24, 2008.

[C27] M. Brikas, G. Račiukaitis and **M. Gedvilas**, *Accumulation effects during processing of metals and silicon with repetition-rate lasers*, "The 11th Nordic Conference in Laser Materials Processing" (11-NOLAMP), Lappeenranta, Finland, August 20-22, 2007.

[C28] G. Račiukaitis, M. Brikas, **M. Gedvilas** and G. Darčianovas, *Patterning of ITO on glass with picosecond lasers for OLED's*, "International Congress on Applications of Lasers & Electro-Optics" (ICALEO 2006), Scottsdale, USA, October 30 - November 2, 2006.

[C29] **M. Gedvilas**, G. Račiukaitis, M. Brikas and G. Darčianovas, *Structuring of ITO layer on glass with high repetition rate picosecond lasers*, Short course "Advanced laser processing in Photonics: State of the Art and Prospects", Heraklion, Crete, Greece, October 26-27, 2006.

[C30] G. Račiukaitis, K. Regelskis, M. Brikas, **M. Gedvilas** and E. Stankevičius, *Interaction of short-pulse-laser radiation with material as a processing method in microscale*, International Conference "Spinduliuotės

sąveika su medžiaga ir jos naudojimas technologijoje 2006", Kaunas, Lithuania, September 28-30, 2006.

[C31] M. Gedvilas and G. Račiukaitis, *Wettability modification of Teflon and silicon surface by using UV picosecond laser radiation*, International Conference "Spinduliuotės sąveika su medžiaga ir jos naudojimas technologijoje 2006", Kaunas, Lithuania, September 28-30, 2006.

[C32] G. Račiukaitis, M. Brikas, **M. Gedvilas** and T. Rakickas, *Patterning of Indium-Tin Oxide on Glass with Picosecond Lasers*, "5th International Conference on Photo-Excited Processes and Applications" (5-ICPEPA), Charlottesville, Virginia, USA, September 3-7, 2006.

[C33] G. Račiukaitis, M. Brikas, **M. Gedvilas** and G. Darčianovas, *Patterning of ITO with Picosecond Lasers*, International Conference "Advanced Optical Materials and Devices" (5-AOMD), Vilnius, Lithuania, August 27-30, 2006.

[C34] G. Račiukaitis, M. Brikas, **M. Gedvilas** and G. Darčianovas, *Structuring of ITO layer on glass with high repetition rate picosecond lasers*, The 4th International Congress on "Laser Advanced Materials Processing" (LAMP 2006), Kyoto, Japan, May 16-19, 2006.

[C35] M. Gedvilas and M. Brikas, *Lazerinės abliacijos skaitmeninis modeliavimas*, VGTU Lietuvos IX-oji jaunųjų mokslininkų konferencija „Fizika ir fizinė kompiuterija", Vilnius, Lithuania, April 7, 2006.

[C36] M. Gedvilas and G. Račiukaitis, *Investigation of UV picosecond laser ablation of polymers*, EPIC/SPIE "Workshop on Laser Applications in Europe", Dresden, Germany, November 23-24, 2005.

[C37] G. Račiukaitis and **M. Gedvilas**, *Processing of Polymers by UV Picosecond Lasers*, "24th International Congress on Applications of Lasers & Electro-Optics" (ICALEO 2005), Miami, USA, October 31 - November 3, 2005.

[C38] M. Gedvilas, *Visuotinės traukos dėsnio pataisa kaip alternatyvus tamsiosios materijos problemos sprendimas*, Vilniaus universiteto Fizikos fakulteto IV-oji studentų mokslinė konferencija "Laisvieji skaitymai 2002", Vilnius, Lithuania, April 19, 2002.

1.5 CONTRIBUTIONS

1.5.1 Author's contribution

The author of the thesis consulting with the scientific supervisor developed the theoretical part and participated in the experimental part of the study. His contribution included:

1. Development of experimental setup and research methods, programming of experiments;
2. Visualization, modeling, interpretation and preparation for publication of the experimental results;
3. Preparation of methodology of grating characterization;
4. Writing scientific publications and presentation of the results on conferences;
5. Supervision of students B. Voisiat and S. Grubinskas in the Project „Promotion of Students Scientific Activities" (Studentų mokslinė praktika) and V. Kučikas in the Project „Student Scientific Research" (Studentų moksliniai tyrimai) involved in the experimental work and simulations of processes in thin metal films under laser irradiation.

1.5.2 Coauthors' contribution

Dr. K. Regelskis together with Dr. Gediminas Račiukaitis were the first who experimentally discovered the ripple formation in thin chromium film under irradiation with an elliptically shaped nanosecond laser pulse. They patented this phenomenon in The State Patent Bureau of the Republic of Lithuania as a possible method of diffraction grating fabrication [15]. It was the starting point for my research in order to understand the processes involved in the ripple formation and to find out means to control the grating parameters.

Some experimental and modeling work was done by students under my supervision. Experiments on possible ripple formation in different metal films were performed by B. Voisiat. Modeling of the free surface flow in liquid film

using COMSOL Multiphysics software was performed by S. Grubinskas and V. Kučikas.

2 LITERATURE REVIEW

2.1 LASER-INDUCED PERIODIC SURFACE STRUCTURES AND RIPPLE TYPES

Development of laser-induced periodic surface structures (LIPSS), or ripples, was discovered shortly after invention of the laser and has been studied experimentally ever since 1965 [17]. The first, widely accepted theoretical approach describing LIPSS suggested that the structures result from an interference of the incoming laser beam with surface-scattered electromagnetic waves [18, 19]. In general, this theory was successful in description of uniformly distributed patterns with the periodicity dependent on the laser wavelength and on the angle of incidence [17, 19-21]. These ripples were aligned perpendicularly to the direction of polarization of the laser light and had a period in the order of several hundreds of nanometers [20, 22]. The period of the structures, was dependent on the wavelength, of the laser radiation, the refractive index, of the irradiated material and the angle of incidence beam to the sample [23].

2.1.1 Interference between an incident beam and surface scattered waves

In the most common type of surface topography, with a period close to the wavelength λ of the laser radiation was observed. This has been attributed to interference between the incident laser radiation and scattered or excited surface waves [20, 22, 24-32]. Spacing Λ between the ripples changes if the incident laser radiation has an inclination θ to the surface normal. The equation for Λ can be expressed for the *p*-polarized beam in reflection [20]:

$$\Lambda = \frac{\lambda}{1 \pm \sin\theta}, \tag{1}$$

in refraction [23]:

$$\Lambda = \frac{\lambda}{n \pm \sin\theta}, \tag{2}$$

where n is the refractive index of the irradiated material, the plus and the minus refer to the downwards and upwards running surface waves on the inclined surface. In most cases, the ripple orientation was found to be perpendicular to the polarization of the incident beam (see Fig. 1a). For the *s*-polarized beam another type of equation should be used in reflection [20]:

$$\Lambda = \frac{\lambda}{\cos\theta}, \tag{3}$$

in refraction [33]:

$$\Lambda = \frac{\lambda}{n\cos\theta}. \tag{4}$$

Fig. 1b shows the measured spacing width of the three different types of LIPSS (dots) compared with the angular dependence according to Eqs. (1) and (3) (lines).

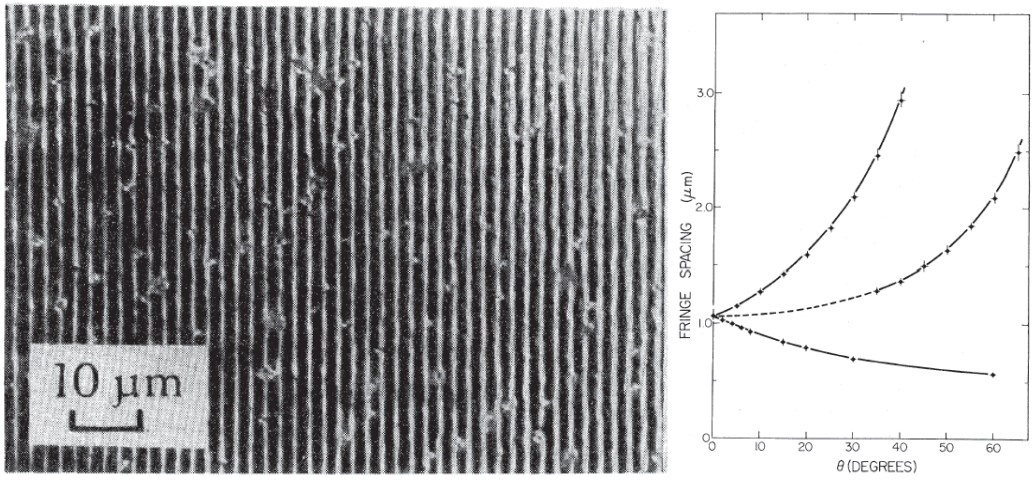

a) b)

Fig. 1 (a) Photograph of ripples produced on bulk Ge surface with radiation of a *p*-polarized nanosecond laser (τ_p = 20 ns) at an angle of incidence of θ = 60°, F_{th} = 50-60 mJ·cm^{-2}, F_0 = 100 mJ·cm^{-2}, $N \approx 30$, (b) Measured spacing of the dominant patterns produced on Ge with the *p*-polarized radiation depending on the angle of incidence θ. The curves are plots of the functions $1.06/(1-\sin\theta)$ (top), $1.06/\cos\theta$ (middle) and $1.06/(1+\sin\theta)$ (bottom) [20].

The LIPSS with periodicity $\Lambda \approx \lambda/n$ were found on the unpolished diamond film by Wu et al. [34] (see Fig. 2) and on fused silica by Böhme et al. [29] treated with a *p*-polarized femtosecond laser beam.

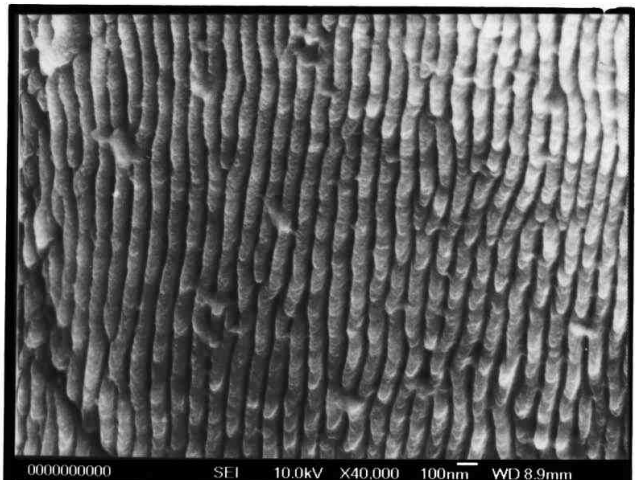

Fig. 2 SEM image of LIPSS on diamond film treated by the laser radiation at a near normal incidence ($\theta = 5°$ *p*-polarized, $\lambda = 400$ nm laser, $F_0 = 0.25$ J·cm^{-2}, $N = 3000$ pulses) [34].

The period of LIPSS was parallel to the laser polarization and independent of the angle of incidence. The results were explained by an interference of the incident laser and the surface scattered waves related to the excited electrons during laser interactions with material.

2.1.2 Laser-induced stress-related instabilities in metal films

Spontaneous breakings in axial symmetry imposed by laser beams can result in the star like instability found by Mogyorósi et al. [35] (see Fig. 3).

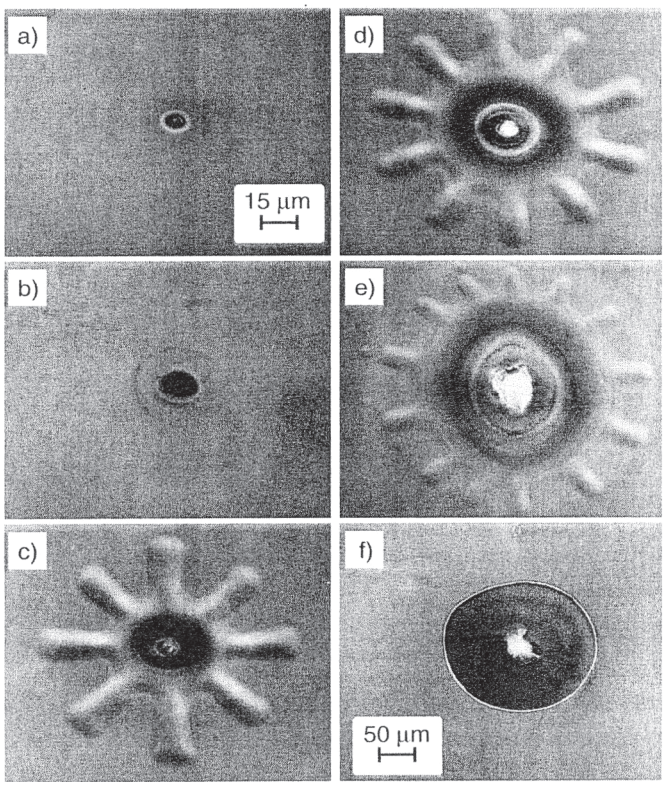

Fig. 3 SEM pictures of holes and stars formed in $h = 250$ nm Mo films on glass during Ar^+ laser-induced etching in Cl_2 atmosphere ($\lambda = 488$ nm, $w_0 = 5.7$ µm ($1/e$), $p(Cl_2) = 50$ mbar). The laser power employed was (a) $P = 10$ mW, (b) $P = 20$ mW, (c) $P = 50$ mW, (d) $P = 100$ mW, (e) $P = 500$ mW, (f) $P = 1500$ mW [35].

Using a low laser intensity for etching, regular holes in Mo films placed in the Cl_2 atmosphere were observed. At medium intensities, a star-like structure developed. The number of rays increased with intensity. The formation of stars was related to build-up stress caused by laser induced heating. Beyond a certain laser light intensity stresses became so high that a large area of the film popped off. This behavior was only observed with the films which were not strongly adhered to the substrate surface.

2.1.3 Instabilities during laser direct writing

Oscillations with a stable (spatial) period much longer than that of the ripples have been observed in diverse laser-direct-write experiments. Formation of a periodical structure induced by an oscillating change in the surface absorptivity and morphology has been observed in tungsten by Kargl et al. [36] (see Fig. 4).

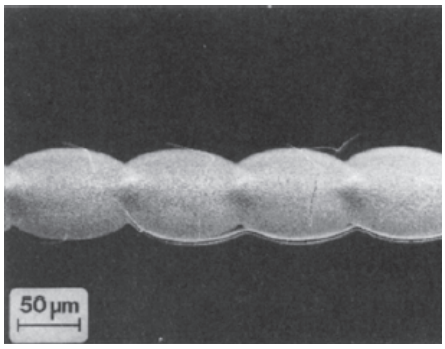

Fig. 4 Periodic structure observed in the line written with a CW Ar^+-laser on a tungsten film (h = 70 nm) on the fused quartz substrate (λ = 514.5 nm, P = 650 mW, $2w_0$ = 15 µm, v = 15 µm·s^{-1}) [36].

These oscillations are neither related to the wavelength and polarization of the laser light nor to the latent heat effects. Their period has been found to increase with the laser power, scanning velocity, size of focus, and pressure of the reactant gas.

2.1.4 Explosive crystallization

Explosive crystallization was observed during laser-induced crystallization of amorphous Si and Ge films on thermally insulating substrates by Chapman et al. [37]. In these systems, the latent heat release related to the structural transformation from amorphous to crystalline exceeded the absorbed laser power and crystallization became self-promoting. If the laser beam was scanned with respect to the substrate, crescent like periodic structures were observed within a narrow, well defined range of scanning velocities (Fig. 5).

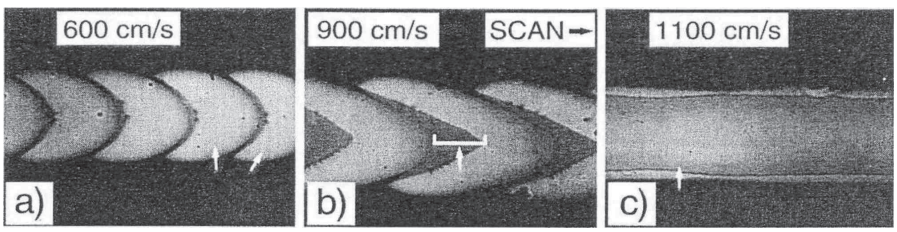

Fig. 5 Optical transmission photographs of laser-crystallized Si lines on Si_3N_4 coated glass substrates for different scanning velocities v [38].

The period of the structure increased with the scanning speed, it also depended on the type of material, the layer thickness, the laser power, and the ambient temperature. During the laser direct writing, the absorbed power ignited the crystallization process whenever it had stopped, and a new cycle started near the edge of the crystallized material. Periodic structures were observed only in a certain range of scanning speed.

2.2 MECHANICALLY AND THERMALLY INDUCED RIPPLES

2.2.1 Marangoni convection in liquid metal

Surface tension γ is a thermodynamic property of a liquid which depends on the temperature and other parameters such as chemical composition and surface cleanliness [39]. If the temperature difference is small, the temperature dependence of γ can be linearized in such a way that $\mathrm{d}\gamma/\mathrm{d}T$ is a constant. It has usually a negative value for liquid metals [40]. When the temperature varies substantially along the free surface, the gradient in surface tension $\mathrm{d}\gamma/\mathrm{d}x$ results in a shear force [41]:

$$\tau = \frac{\mathrm{d}\gamma}{\mathrm{d}x} = \frac{\mathrm{d}\gamma}{\mathrm{d}T}\frac{\mathrm{d}T}{\mathrm{d}x}, \tag{5}$$

which causes fluid to move from the hot region to the cold region as shown in Fig. 6 [42, 43].

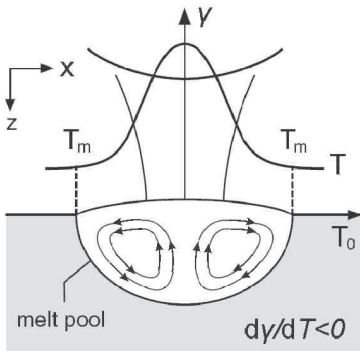

Fig. 6 Schematic cross-section of the melt pool convection during laser melting for $\mathrm{d}\gamma/\mathrm{d}T < 0$ [44].

This phenomenon is called Marangoni or capillary convection and it is characterized by the dimensionless Marangoni number [45, 46]:

$$\mathrm{Ma} = \frac{\mathrm{d}\gamma}{\mathrm{d}T}\frac{\mathrm{d}T}{\mathrm{d}x}\frac{L^2}{\eta\alpha_{\mathrm{diff}}}, \tag{6}$$

where $\mathrm{d}T/\mathrm{d}x$ is the bulk temperature gradient across the domain, $\mathrm{d}\gamma/\mathrm{d}T$ is the temperature coefficient of the surface tension, L is a characteristic length of the surface, η is the dynamic viscosity of fluid and α_{diff} is the thermal diffusivity. The velocity of liquid metal can be calculated using the following equation [47-53]:

$$u = \frac{1}{\eta}\frac{\mathrm{d}\gamma}{\mathrm{d}T}\frac{\mathrm{d}T}{\mathrm{d}x}h, \tag{7}$$

where h is the thickness of liquid metal. In thin films irradiated with the Gaussian beam, the Marangoni flow results in formation of dry areas. Surface tension gradient due to the non-uniform heating induces a flow of the molten liquid away from the center of the irradiated area, leading to formation of dry areas on the substrate [54, 55].

2.2.2 Plateau–Rayleigh instability

A thin jet of a liquid or a non moving cylinder of a fluid are unstable to disturbances with the period larger than $\Lambda > 2\pi R_0$ and break into droplets as shown in Fig. 7. This phenomenon is called the Plateau-Rayleigh instability [56].

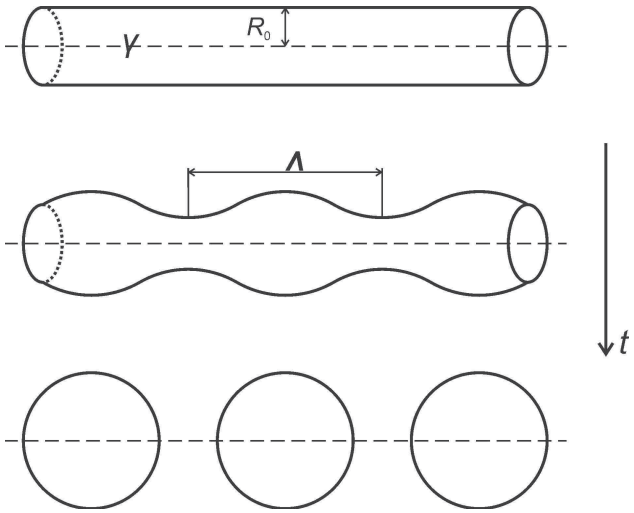

Fig. 7 Plateau-Rayleigh instability. Small perturbations in radius of a liquid cylinder grow in time. The capillarity force drives fluid away from the throat, leading the liquid cylinder to collapse into droplets. R_0 is the radius of the initial un-perturbed cylinder, γ is the surface tension, Λ is the period of the fastest growing mode, t represents the liquid cylinder evolution in time.

The jet changes in its shape in order to reduce the total surface energy. The fastest growing mode occurs when the period of the disturbance is [56, 57]:

$$\Lambda = 9.02 R_0 . \tag{8}$$

The radius of a perturbed cylinder grows exponentially in time until it breaks into droplets. The characteristic time scale is given by [58, 59]:

$$\tau_0 = 2.74 \sqrt{\frac{\rho R_0^3}{\gamma}} , \tag{9}$$

where ρ is the liquid density.

2.2.3 Spinodal dewetting

Thin liquid films generally are not stable. Instabilities in a thin film may lead to rupture, hole formation, and other morphological changes which amplify the non-uniformity in the thin film [60] (see Fig. 8).

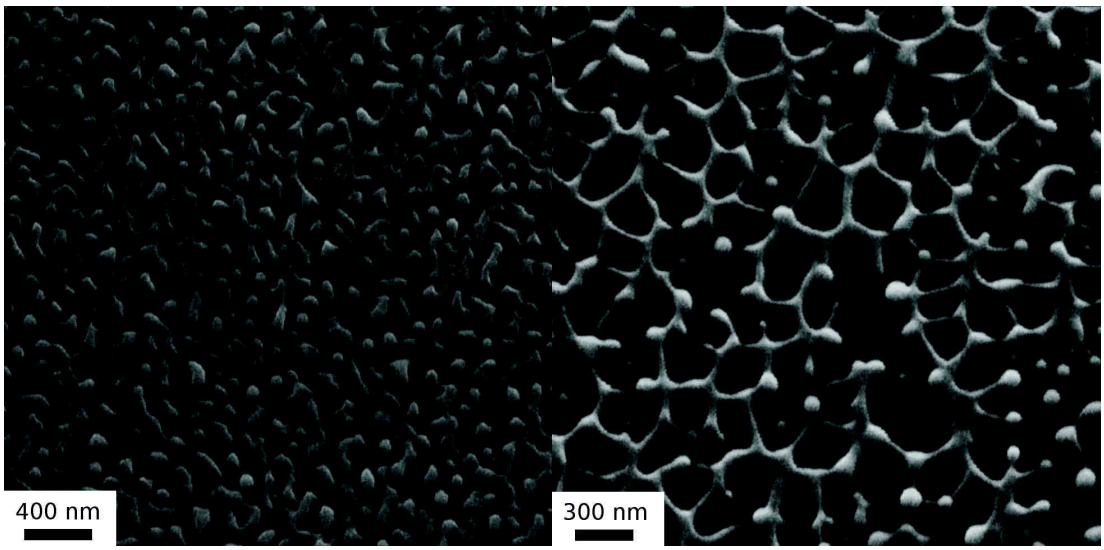

a) b)

Fig. 8 SEM micrographs of the film morphologies after laser irradiation. The Zn and Fe film dewetting due to hydrodynamic instability of thin films. (a) the Zn-film dewetting via a bi-continuous structure. (b) the Fe-film progressing through a polygon-like network [61].

This morphological evolution in an unstable thin film is generally known as dewetting [62]. There are a number of theoretical and experimental studies on dewetting in thin films [63-66]. Spinodal dewetting originates from the surface corrugations which occur due to thermal fluctuations. As a result, at any given moment of time some parts of the film are thinner than initial thickness *h* of the film. Surface tension tends to smoothen the film again. If, however, attractive surface forces exist, the system can gain free energy by thinning the already thinner part even further. Surface forces also act on those parts of the film that are thicker than *h*. Since the surface forces decrease with distance, the effect on the thicker parts is less than that on the thinner parts. This leads to the hole formation and dewetting. The starting point for modeling of the processes is the incompressible Navier-Stokes equation [67]:

$$\begin{aligned} &\rho\left(\frac{\partial \mathbf{u}}{\partial t}+\mathbf{u}\cdot\nabla\mathbf{u}\right)=-\nabla p+\eta\nabla^2\mathbf{u}+\mathbf{f}, \\ &\nabla\cdot\mathbf{u}=0 \end{aligned} \tag{10}$$

where t is the time, where **u** is the fluid velocity, p is the pressure, ρ is the density, η is the dynamic viscosity, and **f** represents the body forces (per unit volume) acting on the fluid. For thin liquid films, Eq. (10) simplifies to the lubrication approximation equation [67-73].

$$\frac{\partial h}{\partial t} = -\frac{1}{3\eta}\nabla\cdot\left(\gamma h^3\nabla\nabla^2 h + \frac{A_{\mathrm{H}}}{2\pi h}\nabla h\right), \tag{11}$$

where γ is the surface tension, A_{H} is the Hamaker constant, $\nabla^2 h$ is the approximation of the surface curvature, and $\left(A_{\mathrm{H}}/2\pi h\right)\nabla h$ is the consequence of the dispersion forces. Such film is unstable with respect to fluctuations larger than a critical and the fastest growing period [41, 61]:

$$\Lambda = h^2\sqrt{\frac{8\pi^3\gamma}{A_{\mathrm{H}}}}\,. \tag{12}$$

This characteristic mode grows faster than all modes and dominates in the emerging dewetting pattern. The characteristic formation time is given by [41, 61]:

$$\tau_0 = \frac{48\pi^2\gamma\eta}{A_{\mathrm{H}}^2}h^5\,. \tag{13}$$

The pattern formation taking place during dewetting can also be of great importance in nanotechnology, with the possibility of designing patterned surfaces for specific applications, e.g., for preparing quantum dots [74], nano-rings [75], etc.

2.2.4 Saffman-Taylor instability

The Saffman-Taylor instability arises, or may arise, when two fluids of different viscosity are pushed by a pressure gradient through the Hele-Shaw cell or drained through such a cell under their own weight. This system is unstable because any small perturbation at the interface between two liquids grows in time as shown in Fig. 9.

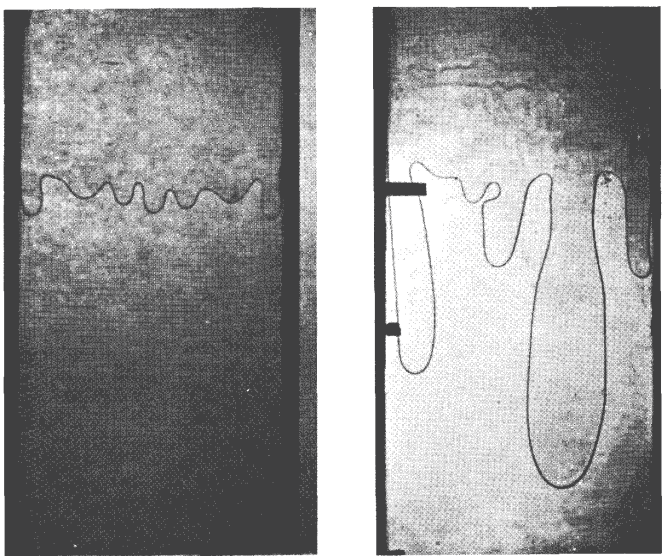

a) b)

Fig. 9 Glycerin in the vertical Hele-Shaw cell. The mean downwards velocity of the two fluids was 1 mm·s^{-1}: (a) an early stage in development of the instability; (b) a later stage in a different experiment [76].

The perturbations with the highest growing speed have a period described by the following equation [56, 77]:

$$\Lambda = \pi h \sqrt{\frac{\gamma}{v\eta}}, \tag{14}$$

where h is the distance between the walls in the Hele-Shaw cell, γ is the surface tension, v is the moving speed, η is the viscosity of liquid.

2.2.5 Fingering instability

The fingering instability of a moving gas-liquid-solid contact line, driven by gravity or thermo-capillarity, has been observed experimentally and studied theoretically [78-83]. The contact line region is usually formed by a sharp moving front between two domains – a thick bulk film and a thin precursor film. The contact line instability is caused by the formation of a ridge on this front which becomes unstable due to a mechanism analogous to the Plateau-Rayleigh instability of the liquid cylinder described previously. The example

of the ascending Marangoni film formed by applying thermal gradient along the vertical surface is shown in Fig. 10.

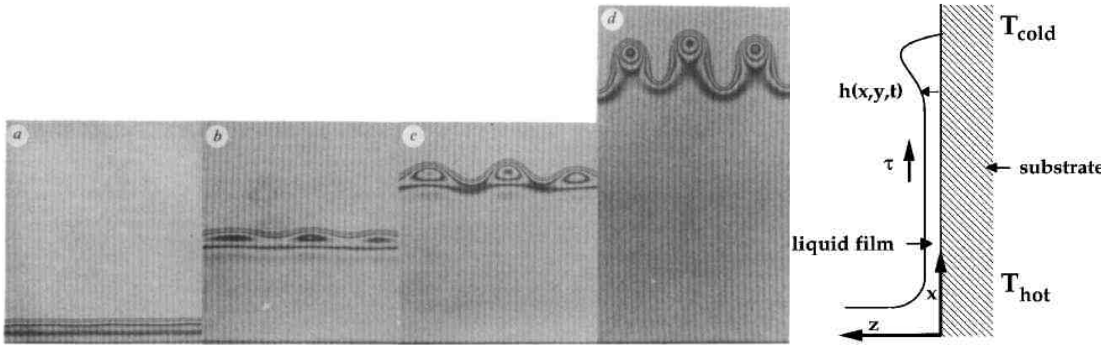

a) b) c) d) e)

Fig. 10 Time development of the fingering instability at a vertical ascending form of a PDMS oil film viscosity $\eta = 20$ mPa·s^{-1} and shear stress $d\gamma/dx = 0.18$ Pa. (a) 1.5 min; (b) 6.5 min; (c) 10 min; (d) 17 min. The measured tip-to-tip period in (d) is $\Lambda = 0.5$ mm [78]. (e) Schematic of spreading geometry for vertically climbing films [84].

A characteristic ratio of the period of the fingering instability to capillarity length predicted theoretically and observed experimentally is [78, 84]:

$$\Lambda / L_0 = 18 - 25, \tag{15}$$

where L_0 is the length of capillarity region [78, 85]:

$$L_0 = h\left(\frac{3\eta u}{\gamma}\right)^{-1/3}, \tag{16}$$

the formation time [78, 81]:

$$\tau_0 = L_0 / u, \tag{17}$$

where u is the capillarity speed.

2.2.6 Buckle morphology of compressed films

Surface films and coatings, that have a higher thermal expansion coefficient than a substrate, often sustain substantial compressive stresses when heated with the laser pulse. These surface layers are susceptible to a buckling-driven

delamination if the interface has low toughness [86]. Various shapes of buckled region are observed, including long straight-sided blisters, circular blisters, and the so-called phone-cord blister.

Thin layers may buckle and delaminate periodically from a substrate when subjected to a compressive strain (see Fig. 11).

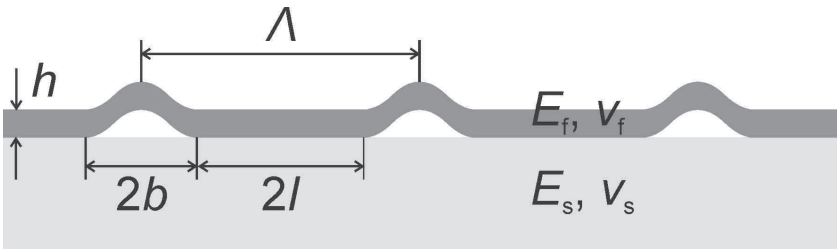

Fig. 11 The film-substrate system with the buckled film, h is the film thickness, Λ is the period of buckle morphology, E_f, E_s, ν_f, ν_s are the Young's modulus and Poisson's ratio of film and substrate respectively, b is the half of buckle width, l is the characteristic length of adhered film.

The period of the buckle morphology is given by:

$$\Lambda = 2(l+b). \tag{18}$$

For an elastic layer attached to a rigid substrate, assuming the layer is clamped at its edges, the critical buckling strain is given by the Euler equation [87, 88]:

$$\varepsilon_{c\,grid} = \frac{\pi^2}{12}\left[\frac{h}{b}\right]^2. \tag{19}$$

Apart from the mismatch in the thermal expansion coefficient between the layer and the substrate, Dundurs [89] has defined two elastic mismatch parameters which are relevant to the layer buckling and delamination. For our application, the most important one is the first parameter α_D defined for the plane – strain problems as [90]:

$$\alpha_D = \frac{E'_f - E'_s}{E'_f + E'_s}, \tag{20}$$

here E' is the plane–strain Young's modulus $E'=E/(1-\nu^2)$, E is the Young's modulus and ν indicates the Poisson's ratio. Note that for an elastic layer on a rigid substrate $\alpha_D \to -1$, for a homogenous elastic system $\alpha_D = 0$, and for a stiff

layer on a compliant substrate $\alpha_D \rightarrow +1$. This width scales with a characteristic length l [91]:

$$l = \frac{2h}{\left[1-\alpha_D\right]}. \tag{21}$$

2.2.7 Periodical thin film fracture

The thermal expansion in solids is given by [92]:

$$\varepsilon = \beta \cdot \Delta T, \tag{22}$$

$\varepsilon = \Delta l / l$ is the strain, β is the linear thermal expansion coefficient, ΔT is the temperature difference. The thermal expansion mismatch is [93]:

$$\varepsilon_f = \left(\beta_f - \beta_s\right) \cdot \Delta T. \tag{23}$$

The misfit stress in the film [93-97]:

$$\sigma_f = \frac{\varepsilon_f E_f}{1-\nu_f}. \tag{24}$$

More accurate results on the thin-film stress on a substrate were achieved by Veiko [98] and agree well with Eq. (24) for a thick substrates. The strain induced by the laser thermal heating [99]:

$$\frac{\Delta l}{l} = \beta \frac{F_0\left(1-R\right)}{L\rho C_p} = \frac{\beta\left(1-R\right)F_0}{\left(\kappa\rho C_p \tau\right)^{1/2}}. \tag{25}$$

Fracture of chromium on fused silica was observed experimentally after laser irradiation [99] when the strain induced by laser radiation calculated using Eq. (25) exceeded the strain at rupture. Periodical cracking was described firstly [100] and later periodical cracking stress equation was derived [101-103]. Fig. 12 illustrates the cracking at 11 % strain. The average crack spacing for the 100 nm-thick chromium thin film is 4.1 μm [104].

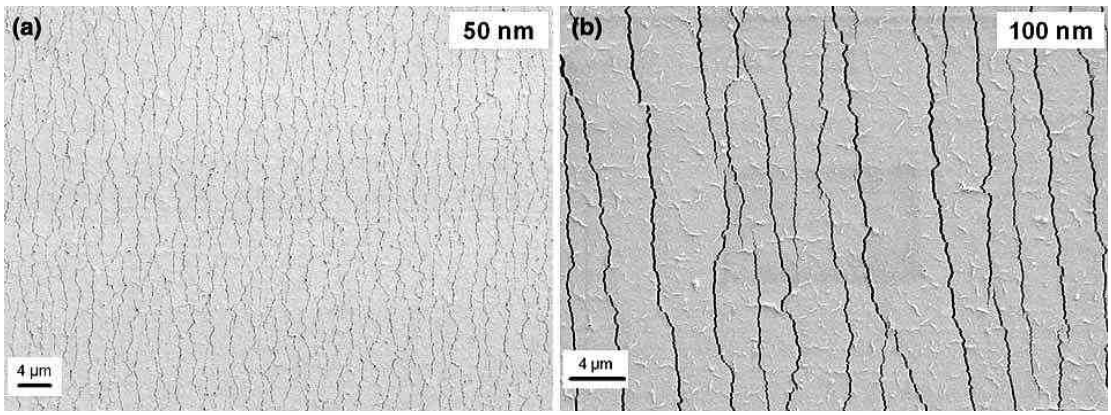

Fig. 12 The SEM micrographs at the same magnification of the films strained to 12 %. The effect that thickness has on the crack spacing as well as the first stages of buckling in the film are evident: Thickness of the film: (a) 50 nm; (b) 100 nm [104].

This leads to defining the maximum shear traction supported by the interface, $\tau_{\max}$, as a function of the fracture stress of the film, σ_{frac}, as

$$\tau_{\max} = \frac{3\pi h}{4\Lambda}\sigma_{\text{frac}}, \tag{26}$$

where h is the film thickness and Λ is the mean spacing between cracks. Similar equation was given in [105]. The fracture stress can be estimated from Eq. (26), assuming that the film behaves elastically,

$$\sigma_{\text{frac}} = E\varepsilon_{\text{frac}}, \tag{27}$$

where E is the elastic modulus of the film and $\varepsilon_{\text{frac}}$ is the fracture strain. It should be noted that Eq. (27) does not take into account the residual in-plane stress of the film after deposition [104].

2.3 LIGHT MATTER INTERACTION

2.3.1 Absorption of laser radiation

The reflection at the surfaces is described by the coefficient of reflection or reflectivity. This is usually given by the symbol R_λ and is defined as the ratio of the reflected power to the power incident on the surface. The coefficient of transmission or transmittance T_λ is defined likewise as the ratio of the

transmitted power to the incident power. If there is no scattering, then by conservation of energy [106]:

$$A_\lambda + R_\lambda + T_\lambda = 1, \tag{28}$$

where A_λ is the absorptivity. The absorption and refraction of a medium can be described by a single quantity called the complex refractive index. This is usually given by the symbol $\tilde{n}$ and is defined through the equation:

$$\tilde{n} = n + ik. \tag{29}$$

The real part of the complex refractive index, namely n, is the same as the normal refractive index. The imaginary part of $\tilde{n}$, namely k, is called the extinction coefficient. The reflectivity depends on both n and k and is given by [107]:

$$R_\lambda = \left|\frac{\tilde{n}-1}{\tilde{n}+1}\right|^2 = \frac{(n-1)^2 + k^2}{(n+1)^2 + k^2}. \tag{30}$$

It gives the coefficient of reflection between the medium and the air (or vacuum) at a normal incidence. The absorption of light by an optical medium is quantified by its absorption coefficient α. This is defined as the fraction of the power absorbed in a unit length of the medium. Extinction coefficient k is directly related to the absorption coefficient of the medium [107]:

$$\alpha = \frac{4\pi k}{\lambda}, \tag{31}$$

where λ is the wavelength of light in vacuum. According to the Beer–Lambert–Bouguer law the intensity of the electromagnetic wave inside a material decays exponentially. If the beam is propagating in z direction, and the intensity (optical power per unit area) at position z is $I(z)$, then the decay of the intensity inside a material can be expressed as [107]:

$$I(z) = I_0 e^{-\alpha z}, \tag{32}$$

where I_0 is the intensity of the incident beam. The transmittance of an absorbing medium of at distance z is given by:

$$T_\lambda = (1 - R_\lambda) e^{-\alpha z}, \tag{33}$$

and the absorptivity from Eqs. (28) and (33) is:

$$A_\lambda = \left(1 - R_\lambda\right)\left(1 - e^{-\alpha h}\right). \tag{34}$$

The penetration depth [108, 109]:

$$\delta_{\mathrm{p}} = \frac{1}{\alpha}, \tag{35}$$

is the parameter that describes the decay of electromagnetic waves inside the material. It refers to the depth at which the intensity or power of the field decays to e^{-1} (about 37%). The skin depth $\delta_{\mathrm{e}} = 2\delta_{\mathrm{p}}$, twice as large as penetration depth refers to the length from the surface at which the magnitude of the electric (or magnetic) field has decayed to e^{-1} of its surface value [110]. The skin depth is also known as a length at which the power of the wave has decreased to e^{-2} or about 13% of its surface value.

2.3.2 Heat transfer equation

The laser power absorbed by material finally is converted to heat. The time-dependent temperature distribution at the target depth $T(t, z)$ is governed by the heat flow equation in one-dimensional form, appropriate to many experimental situations [111-113]:

$$\frac{\partial T}{\partial t} = \alpha_{\mathrm{diff}} \frac{\partial^2 T}{\partial z^2} + \left(1 - R_\lambda\right) \frac{\alpha}{\rho C_p} I\left(t\right) \exp\left(-\alpha z\right) \tag{36}$$

where ρ is the density, C_{p} is the specific heat, T is the temperature, t is the time, z is the longitudinal coordinate, R_λ is the reflectivity, α is the absorption coefficient, $I(t)$ is the laser intensity, α_{diff} is the thermal diffusivity:

$$\alpha_{\mathrm{diff}} = \frac{\kappa}{\rho C_{\mathrm{p}}}, \tag{37}$$

where κ is the thermal conductivity. The two-temperature model (TTM) [114-118] is needed when the laser pulse duration is less than the phonon-electron interaction time which for metals is of the order of 1 ps [119, 120]. When a fs-laser pulse incidents onto surface of a metal sample, it is generally believed that a certain amount of pulse energy will initially deposit into the sample over the skin depth across the entire beam spot. During the fs-laser pulse and metal

interactions, the absorbed energy is coupled to electrons and leads to an elevated electron temperature. Subsequently, hot electrons are losing energy through two competing processes, coupling to the cold lattice and diffuse to a lower-temperature region. This electron lattice process can be described by TTM. Heat diffuses away from an irradiated region of a material to a characteristic length described as [121, 122]:

$$D_{\mathrm{haz}} = \sqrt{\alpha_{\mathrm{diff}} \tau_{\mathrm{p}}}\,, \tag{38}$$

where τ_{p} is the laser pulse duration.

2.3.3 Ablated crater diameter and hole depth

For a Gaussian beam, the lateral precision of ablation depends on several laser- and material-related parameters. A simple relationship can be derived between the diameter D of an ablated crater, the material dependent surface damage threshold fluence F_{th}, the Gaussian beam radius w_0 (e^{-2}), and the peak fluence in the beam F_0 [123-125]. This treatment assumes that there is no significant lateral heat conduction. For a Gaussian beam, the spatial fluence profile is given by:

$$F(r) = F_0 e^{-2r^2/w_0^2}\,, \tag{39}$$

where r is the distance from the beam centre, w_0 is the radius of the focused laser beam [126]:

$$w_0 = \frac{4\mathrm{M}^2 \lambda}{\pi} \frac{f}{w}\,, \tag{40}$$

where M^2 is the beam quality parameter, λ is the wavelength, f is the focal length of the objective, w is the beam radius on the focusing lens. The peak fluence and the pulse energy, E_{p}, are directly related by:

$$F_0 = \frac{2E_{\mathrm{p}}}{\pi w_0^2}\,. \tag{41}$$

Finally, it can be shown that for the ablation threshold F_{th} and the diameter D of an ablated crater are related to the peak fluence by:

$$D^2 = 2w_0^2 \ln \frac{F_0}{F_{th}}. \tag{42}$$

Because of the linear dependence of the peak laser fluence on the pulse energy, it is possible to determine the beam radius w_0, from a plot of the square of the crater diameters D^2 versus the logarithm of the laser pulse energy E_p (the slope = $2w_0^2$) [123]. It is possible to convert the laser pulse energy E_p to the peak fluence in the beam using Eq. (41). By extrapolation of D^2 back to zero, a value for the ablation threshold fluence F_{th} can be obtained. The ablation depth per pulse logarithmically depends on the laser fluence [127, 128]:

$$d = \frac{1}{\alpha_{eff}} \ln \frac{F}{F_{th}}. \tag{43}$$

It has been shown that there are two different ablation regimes. In both cases the ablation depth per pulse logarithmically depends on the laser fluence. When operating in the first ablation regime, the ablation rate is low and is dependent on the optical penetration depth [129]. While in the second ablation regime, the ablation rate is higher and is characterized by the „electron heat diffusion length" or the „effective heat penetration depth".

2.4 LASER-INDUCED STRUCTURES IN CHROMIUM FILM

The surface morphology of chromium films irradiated at different fluences with a single laser pulse of an excimer laser was investigated by Lee et al. [130]. Nucleation of holes in the metal film took place at low fluences, when some metal layer remained on the substrate. The behavior of the film ablation process was described using three threshold values. Cracking of the film was described by the damage threshold. The chromium film started to melt at the melting threshold. The melting always commenced along the cracks. The glass surface was exposed due to the surface tension of molten chromium. The further increase of the laser fluence led to the film surface modification from net-like shape to irregular long islands and micro-sized small droplets. Finally,

the chromium film was removed completely with a single shot at the complete removal threshold.

The ablation characteristics of the thin chromium film on quartz with double pulses of a femtosecond laser were investigated by Ohmura et al. [131]. Two types of laser ablation for double-pulse irradiation were found. One was the normal ablation involving formation of the ablation front. The other was the fracturing ablation, whose mechanism was considered as follows: the first pulse irradiation with energy close to the ablation threshold yielded to porous structure in the vicinity of the surface. When the second pulse was irradiated to the activated area with a porous structure, the fracturing ablation occurred.

Ultrafast lasers ablation of the Cr film by using double-pulse method was also investigated by Han et al. [132]. Microbump structures were formed on the surface of Cr film after ablation with double ultrafast pulses. Height of the structure exhibited a drop when a delay between double pulses was 1 to 10 ps, which is comparable with the electron–phonon coupling process according to the numerical TTM simulation.

Damage mechanism and morphology characteristics of chromium film in a femtosecond laser rear-side ablation were investigated by Wang et al. [133]. The film removing process included two key sub-processes: the laser ablation and subsequent dynamic process of breaking and ejecting. Film morphology in the rear-side ablation was determined by the interrelation between the laser energy and the film strength. When a lower laser energy was used, a residual film tended to break into some large fragments, which resulted in an irregular ablation shape. While when a higher pulse energy was used, the residual film was broken into small fragments, and the ablation quality improved.

Surface ripple formation during the Cr film ablation with a train of double ultrashort laser pulses was investigated by Kim et al. [10, 134]. Laser irradiation of a metal surface with multiple pulses just below the ablation threshold generated periodic surface patterns - LIPSS. The ripples generally were aligned perpendicularly to the polarization direction of the electric field with a period equal approximately to a half of the wavelength of the light.

Excimer lasers were used for self-formation of metal nanopillars in the chromium film on quartz by nanosecond pulse laser melting [135]. A porous structure was observed in the chromium film after the femtosecond pulse irradiation close to the ablation threshold [136]. Brittle Cr films ruptured before melting and therefore the brittle – ductile transition process must be included in the energy balance [137].

2.4.1 Chromium ablation with an astigmatic beam

The direct laser writing of graduation lines in Cr thin films on glass substrates was investigated by Kopac et al. [138]. The Nd:YAG laser and the astigmatic optical system were used to write rectangular holes in the Cr film (Fig. 13).

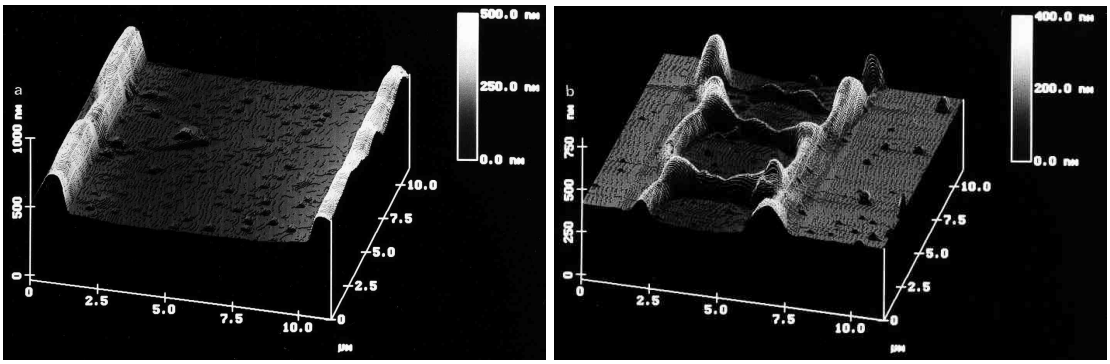

a) b)

Fig. 13 AFM pictures of the graduation lines for different writing parameters. The region of the removed material can be found in the middle of the AFM picture. At the edges of these regions, the rims of resolidified Cr can be seen. The writing parameters: (a) E_p = 230 μJ, h = 40 nm; (b) E_p = 140 μJ, h = 40 nm [138].

The evaporation is concluded to be the essential process in the laser writing of graduation lines. The rims formed by the surface tension gradient at the hole edges indicate that the laser writing of graduation lines is a typical two-phase removal process.

2.5 PHYSICAL PROPERTIES OF CHROMIUM

Chromium is a lustrous, brittle, hard metal. Its color is silver-gray and it can be highly polished. It does not tarnish in air, when heated it burns and forms the green chromic oxide. Chromium is unstable in oxygen, it immediately produces a thin oxide layer that is impermeable to oxygen and protects the metal below [98]. Ion-irradiation of sputtered Cr thin films results in relaxation of tensile stress and build up of compressive stress [139].

Table 1 Properties for chromium at room temperature.

Property	Symbol	Value	Unit	Reference
Hamaker constant	A_H	2.1×10^{-19}	J	[140]
Specific thermal capacity	C_p	23.4	$J\cdot mol^{-1}\cdot K^{-1}$	[141]
Young's modulus	E	280	GPa	[142]
Heat of fusion	L_m	21	$kJ\cdot mol^{-1}$	[143]
Heat of vaporization	L_v	340	$kJ\cdot mol^{-1}$	[143]
Molar mass	M	52	$g\cdot mol^{-1}$	[144]
Reflectivity (λ = 1064 nm)	R_λ	0.58	-	[145]
Melting point	T_m	2180	K	[143]
Boiling point	T_v	2944	K	[143]
Molar volume	V	7.23	$cm^3\cdot mol^{-1}$	[142]
Absorption coefficient (λ = 1064 nm)	α	42	μm^{-1}	[145]
Thermal expansion coefficient	β	4.9×10^{-6}	K^{-1}	[146]
Surface tension	γ	1780	$mN\cdot m^{-1}$	[147]
Surface tension thermal coefficient	$d\gamma/dT$	-0.544	$mN\cdot m^{-1}\cdot K^{-1}$	[147]
Dynamic viscosity (at melting point)	η	4.86	mPa·s	[148]
Thermal conductivity	κ	94	$W\cdot m^{-1}\cdot K^{-1}$	[130]
Density	ρ	7190	$kg\cdot m^{-3}$	[149]
Liquid density (at melting point)	ρ_m	6300	$kg\cdot m^{-3}$	[141]
Poisson's ratio	υ	0.21	-	[150]

The measured fracture strain changes gradually in the temperature range from 300 to 623 K as shown in Fig. 14

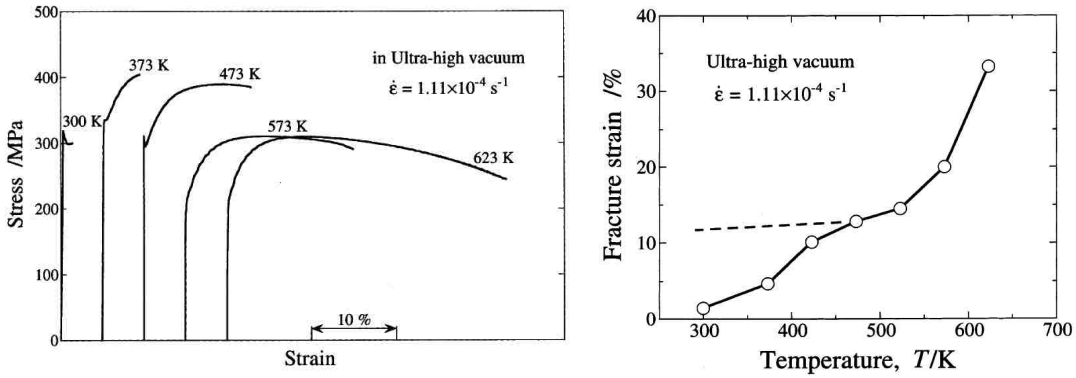

Fig. 14 Stress-strain curves for sintered high purity chromium tested at $T = 300 – 623$ K in ultra-high vacuum (left), temperature dependence of fracture strain of high purity chromium measured in ultra-high vacuum (right) [151].

Several different values of experimental and theoretical ablation threshold of the thin chromium film were obtained by different authors given in Table 2:

Table 2 Ablation threshold of the thin chromium film of the thickness $h = 100$ nm obtained by different groups.

Wavelength, λ [nm]	Pulse duration, τ_p [ns]	Experimental threshold, F_{th} [J·cm^{-2}]	Calculated threshold, F_{th} [J·cm^{-2}]	Reference
248	50	0.7	1.0	[130]
248	14	0.7	0.7	[99]
248	14	0.6	0.5	[152]
1064	7	-	0.8-7.5	[153]

Theoretically the ablation threshold (vaporization) or visible modification (melting) of a thin metal film on a glass substrate can be estimated by simple thermodynamic approach taking into account absorptivity from Eq. (34) [152, 154]:

$$F_{\text{th m}} \approx \frac{\rho h\left[C_{\text{p}}\left(T_{\text{m}}-T_0\right)+L_{\text{m}}\right]}{\left(1-R_\lambda\right)\left(1-e^{-\alpha h}\right)}, \tag{44}$$

where ρ is the film density, h is the film thickness, C_{p} is the specific heat, T_{m} – is the melting temperature, T_0 is the room temperature, L_{m} is the heat of fusion, R_λ is the film reflectivity, α is the absorption coefficient. The vaporization threshold [152, 154]:

$$F_{\text{th v}} \approx \frac{\rho h\left[C_{\text{p}}\left(T_{\text{v}}-T_0\right)+L_{\text{m}}+L_{\text{v}}\right]}{\left(1-R_\lambda\right)\left(1-e^{-\alpha h}\right)}, \tag{45}$$

where L_{v} is heat of vaporization, T_{v} – is the vaporization temperature.

2.6 PHYSICAL PROPERTIES OF METALS

Parameters of liquid metals required for Marangoni coefficient calculation as well as metal film adhesion to the glass substrate are given in Table 3.

Table 3 Metal parameters.

Metal	Surface tension thermal coefficient, $d\gamma/dT$ [$mN \cdot m^{-1} \cdot K^{-1}$]	Dynamic viscosity, η [mPa·s]	Temperature difference, T_{v}-T_{m} [K]	Diffusivity, α_{diff} [$cm^2 \cdot s^{-1}$]	Film adhesion to glass, [a.u.]
Ag	-0.15 [155]	3.5 [40]	1019 [40]	1.74 [156]	8 [157]
Al	-0.19 [158]	1.9 [40]	1400 [40]	0.97 [159]	60-80 [157]
Au	-0.14 [160]	5.5 [40]	1647 [40]	1.27 [161]	2 [157]
Cr	-0.54 [147]	4.7 [40]	295 [40]	0.29 [162]	500 [157]
Cu	-0.18 [155]	4.1 [40]	1547 [40]	1.18 [156]	25-30 [157]

The viscosity of liquid metal can be estimated using Andrade and Dobbs formula [163]:

$$\eta_{\text{m}} \approx C_{\text{A}} M^{1/3} T_{\text{m}}^{1/3} V_{\text{m}}^{-2/3}, \tag{46}$$

where M is the atomic weight, $C_A = 1.8\times10^{-7}\ \mathrm{J^{1/2}\cdot K^{-1/2}\cdot mol^{-1/6}}$ is the Andrade coefficient calculated theoretically. Surface tension of liquid metal at melting point can be achieved using the Allen formula [164]:

$$\gamma_m \approx C_A R^* T_m V_m^{-2/3}, \tag{47}$$

where T_m is the absolute temperature of melting point, V_m is the atomic volume at T_m, $R^* = 8.31\ \mathrm{J\cdot mol^{-1}\cdot K^{-1}}$ is the gas constant, $C_A = 4.8\times10^{-8}\ \mathrm{mol^{1/3}}$ is the Allen constant. The relationship between surface tension and absolute temperature is the Eötvös law which can be expressed in the form [40, 164].

$$\gamma = \frac{k_y}{V^{2/3}}\left(T_c - T\right), \tag{48}$$

where $k_y = 6.4\times10^{-8}\ \mathrm{J\cdot K\cdot mol^{2/3}}$ for liquid metals, T_c is the critical temperature, where the surface of liquid phase and gas phase disappears, introduced by Grosse [44]. The temperature coefficient of the surface tension:

$$\frac{\mathrm{d}\gamma}{\mathrm{d}T} = \frac{k_y}{V^{2/3}}\left[\frac{2\left(T_c - T\right)}{3\rho}\frac{\mathrm{d}\rho}{\mathrm{d}T} - 1\right]. \tag{49}$$

Good agreement of experimental and theoretical surface tension coefficients was found for the majority of liquid metals [40].

2.7 PHYSICAL PROPERTIES OF GLASS

The physical properties of glass are given in Table 4:

Table 4 Properties of glass at room temperature [62].

Property	Symbol	Value	Unit
Young's modulus	E	70	GPa
Poisson's ratio	υ	0.23	-
Thermal expansion coefficient	β	9.1×10^{-6}	$\mathrm{K^{-1}}$
Density	ρ	2500	$\mathrm{kg\cdot m^{-3}}$
Specific thermal capacity	C_p	720	$\mathrm{J\cdot kg^{-1}\cdot K^{-1}}$
Thermal conductivity	κ	1	$\mathrm{W\cdot m^{-1}\cdot K^{-1}}$

3 EXPERIMENTAL SET-UPS AND PROCEDURES

Material related to this chapter was published in [A4], [A5] and [C8], [C9].

3.1 EXPERIMENTAL SET-UP

Experiments on the laser ablation were performed using the diode pumped nanosecond Nd:YAG laser NL202 (Ekspla Ltd.) with the Gaussian intensity profile. The laser generated radiation with the wavelength of $\lambda = 1064$ nm, and the pulse duration was $\tau_p = 9$ ns. The pulse energy was up to $E_p = 2$ mJ. The laser was operating at the pulse repetition rate of $f_{Rep} = 1$ kHz in the regime of the position - synchronized output (PSO), controlled by the positioning system (Aerotech Ltd.). Experimental set-up is shown in Fig. 15. Additionally, some of the experiments were repeated by using the picosecond laser FOXTROT (Ekspla Ltd., $\lambda = 1064$ nm, $\tau_p = 60$ ps, $E_p < 1$ mJ, $f_{Rep} = 1$ kHz).

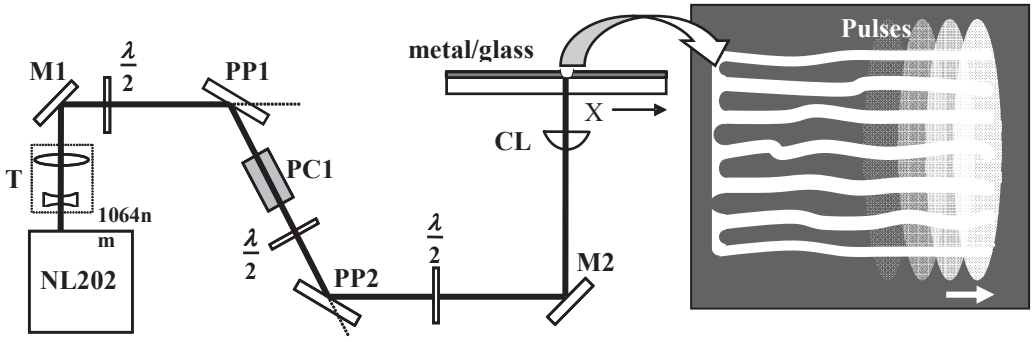

Fig. 15 Scheme of the experimental set-up: NL202 - diode pumped nanosecond laser; T - beam expander; M1, M2 – mirrors; $\lambda/2$ – half-wave phase plate; PP1, PP2 – thin film polarizers; PC1 – Pockels cell; CL - cylindrical lens. Insert on the right shows the process of ripple formation with overlapping pulses.

The laser beam was tightly focused using the acylindrical lens with the focal length of 10 mm. The shape of the lens was specially designed for optimal focusing to a minimal spot through the glass substrate. The laser radiation was focused to the metal film from backside, through the glass

substrate (the rare-side irradiation). The laser spot at the focal position was a high aspect-ratio line with the dimensions of $w_{x0} = 2.5$ μm by $w_{y0} = 2.5$ mm. The spatial energy density distribution in the spot is given by:

$$F(x,y) = F_0 e^{-\frac{2x^2}{w_{x0}^2} - \frac{2y^2}{w_{y0}^2}}, \tag{50}$$

where x and y are the spatial coordinates, F_0 is the peak laser fluence in the center of the beam given by:

$$F_0 = \frac{2E_p}{\pi w_{x0} w_{y0}}, \tag{51}$$

where E_p is the laser pulse energy.

The thin metal films of aluminum, chromium, copper, silver and gold were deposited by vacuum evaporation on a float glass substrate. No intermediate layers were used to increase adhesion of metals to glass. The thickness h of the films used in experiments varied from 50 nm to 200 nm. The thickness of the glass substrate was 4.8 mm.

Samples were placed on the high-precision stage ALS25020 (Aerotech Ltd.) and were irradiated with a burst of partially overlapping laser pulses. The distance between overlapping laser pulses (shift) was precisely controlled with the motion controller and PC. Motion of the stage at a low positioning speed was tested with the ZMI 7702 interferometer (Zygo). It was possible to set the shift between pulses as small as 10 nm.

Morphological investigations of the structures were performed using an optical microscope, AFM and SEM.

3.2 EXPERIMENTAL ABLATION THRESHOLD OF THIN METAL FILMS

The ablation thresholds of thin chromium films were experimentally measured by a simple technique proposed by [123]. The diameters of craters ablated with different laser pulse energies were measured and the threshold fluences were determined from linear fit of experimental data points (see Fig. 16).

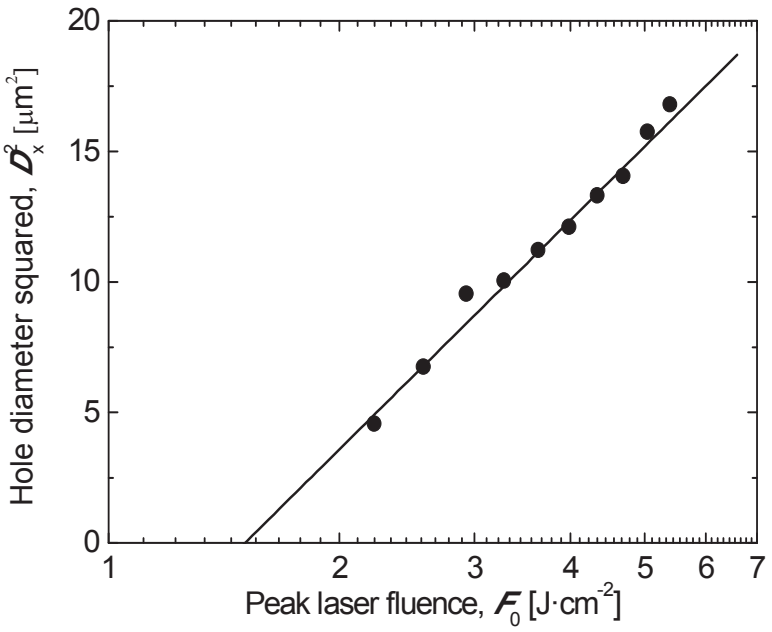

Fig. 16. The squared diameter D_x^2 of the ablated elliptical spot in the thin chromium film on a glass substrate as a function of the peak laser fluence F_0. The solid lines correspond to the linear fit of the experimental data points.

The experimentally measured ablation (removal) threshold of the thin chromium film from the glass substrate thickness h of 100 nm was $F_{th} = 1.51$ J·cm^{-2}. The theoretically calculated energy density required to evaporate the 100 nm thick chromium film off the glass substrate from thermo-physical parameters in Table 1 and Eq. (45) was $F_{th\,v} = 1.41$ J·cm^{-2}. The reason for the smaller theoretical value than experimentally measured value is a local increase of reflectivity during the laser ablation. Similar results were obtained by Matthias et al. [152]. In modeling, the reflectivity might be used as a fitting parameter.

The energy density required for removal of a film from the glass substrate with a single laser pulse was estimated for every material. A plot of the ablated spot diameter versus the laser fluence was used for this purpose. The ablation (film removal) thresholds of the 100 nm thick metal films are presented in Table 5 for all metals used in experiments.

Table 5 The ablation (film removal) threshold F_{th} of metal films with the thickness of 100 nm on the glass substrate.

Metal film	Ablation threshold, F_{th} [J·cm^{-2}]
Ag	0.74
Al	0.57
Au	1.57
Cr	1.51
Cu	0.88

3.3 GRATING CHARACTERIZATION SET-UP

The diffractive properties of the self-organized gratings were investigated by using a traditional technique [165]. The most regular gratings were chosen for testing their diffractive properties. The characterization was done by using an experimental set-up shown in Fig. 17.

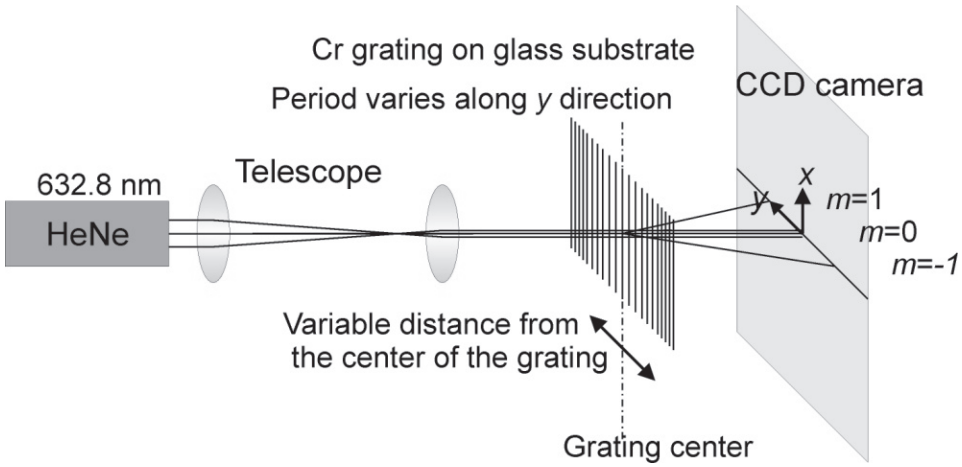

Fig. 17 Experimental set-up for diffraction grating characterization.

The collimated beam of the HeNe laser (wavelength of 632.8 nm) with the beam diameter of ~100 μm on the grating covered a small part of the diffraction grating (width of 2.5 mm). The grating was moved along the *y* axis using the micrometer stage and the interference patterns from various parts of the grating were captured using a CCD camera. The grating period was different in the *y* direction because of difference in energy density whereas the grating was fabricated by using an elliptical spot with the Gaussian distribution in the *y* direction.

4 RIPPLE FORMATION IN THIN CHROMIUM FILM

Material related to this chapter was published in [A3], [A4] and [C4], [C5], [C6].

4.1 FILM ABLATION WITH NON-OVERLAPPING LASER PULSES

The threshold energy density required to remove completely the 100 nm thick chromium film of the glass substrate with a single laser pulse was estimated as $F_{th} = 1.51$ J·cm^{-2}. At this fluence, the central area of the metal film irradiated with a laser beam of Gaussian distribution was evaporated (Fig. 18).

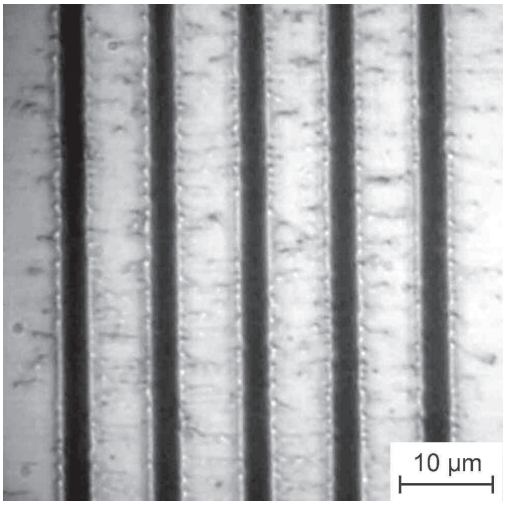

Fig. 18 Picture of five areas cleaned with separate single pulses at laser fluence $F_0 = 2.26$ J·cm^{-2} and shift between them $\Delta x = 10$ µm.

Sharp and smooth edges of the cleaned area were achieved by using the tightly focused laser beam with fluence above the threshold. Variation in width of the area cleaned with a single shot was less than 0.3 µm over the whole length of 2 mm. Ridges of the resolidified metal were always presented on edges of the cleaned area.

4.2 FILM ABLATION WITH OVERLAPPING LASER PULSES

Large areas of the metal film can be removed by superposition of many laser pulses. The optimal conditions for the chromium ablation were investigated experimentally by varying the laser pulse energy and distance between lines ablated with a single laser pulse. The laser beam was focused into the line, and the substrate areas were cleaned by applying many pulses. In a certain range of laser fluences, the partially overlapping pulses formed a complicated structure made of the remaining metal. Ridges formed on edges of the cleaned area affected the behavior of the metal under further irradiation with overlapping pulses.

4.2.1 Quasi-periodical fracture

At a low fluence, below the ablation threshold, the chromium film was cracked, and these cracks were orientated in parallel with the shift direction for the laser pulses (Fig. 19a). When adjacent laser pulses did not overlap sufficiently, the orientation of the rips was rather random (Fig. 19b).

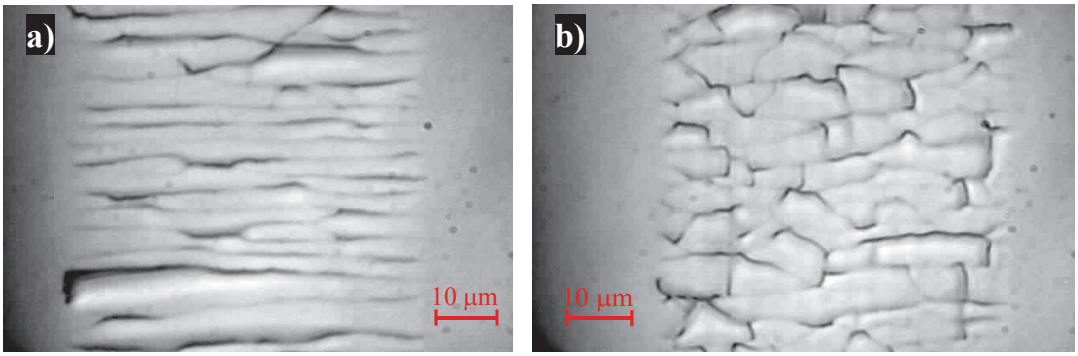

Fig. 19 Cracked surface morphology of the laser-irradiated, 100 nm thick chromium films on the glass substrate: a) F_0 = 1.35 J·cm^{-2}, shift Δx = 0.2 μm; b) F_0 = 1.4 J·cm^{-2}, shift Δx = 1.6 μm. Shift direction of the laser pulses with respect to the sample in all pictures was from the left to the right. The laser spot is oriented vertically in the picture.

As the laser fluence was increased, the chromium film started to melt (Fig. 20). At these laser fluences, the edges of the cracks became softer, and craters of melted chromium were formed between them.

4.2.2 Periodically molten resolidified lines

Melting always began along the cracks. The glass surface was exposed due to the surface tension of molten chromium. When the laser pulse energy was not sufficient to evaporate the whole metal film, the ripples were formed from residues of the melted chromium (see Fig. 20).

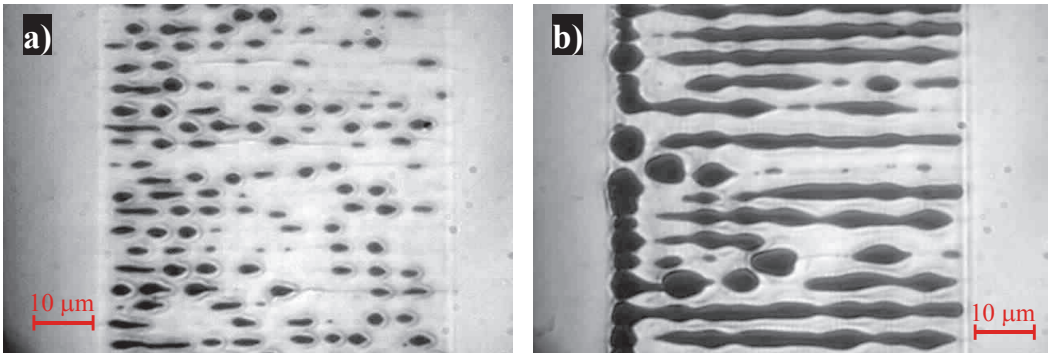

Fig. 20 Cracked and partially melted surface of the laser-irradiated, 100 nm thick chromium films on the glass substrate: a) $F_0 = 1.6$ J·cm^{-2}, shift $\Delta x = 0.4$ µm; b) $F_0 = 1.9$ J·cm^{-2}, shift $\Delta x = 0.8$ µm.

Similar effects of cracking and circular opening formation were found in [130] by irradiation of a wide area of Cr on glass with a single pulse of the excimer laser.

4.2.3 Ripple formation

Fig. 21 shows a picture of ripple structure made with a series of laser pulses starting from the left.

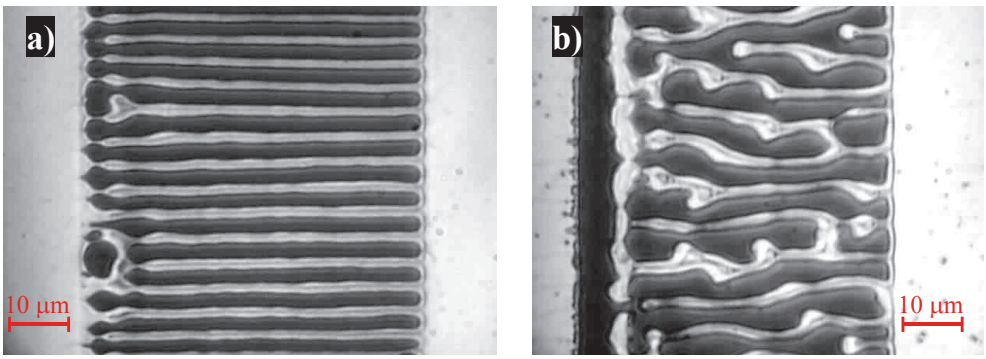

Fig. 21 Ripples formed by partially overlapping pulses on the glass substrate during the processing of the 100 nm thick chromium film: a) regular ripples, $F_0 = 1.9$ J·cm^{-2}, shift $\Delta x = 0.2$ μm; b) irregular ripples, $F_0 = 2.6$ J·cm^{-2}, shift $\Delta x = 0.8$ μm.

The beginning of the ripples on the left was quite irregular, while a periodical grating was composed at the end ripples. The ripples were located periodically (~4 μm) perpendicular to the long axis of the beam spot (in parallel with the laser pulse shift direction). Their direction did not depend on the laser beam polarization.

4.2.4 Initial stage of ripple formation

The dynamics of the ripple formation by irradiation of the film with a sequence of laser pulses is shown in Fig. 22. A linear laser spot was oriented vertically. The first 3-5 overlapping pulses initiated formation of quasi-periodical distribution of ripples perpendicular to the laser spot extent and in line with a shift of the laser beam.

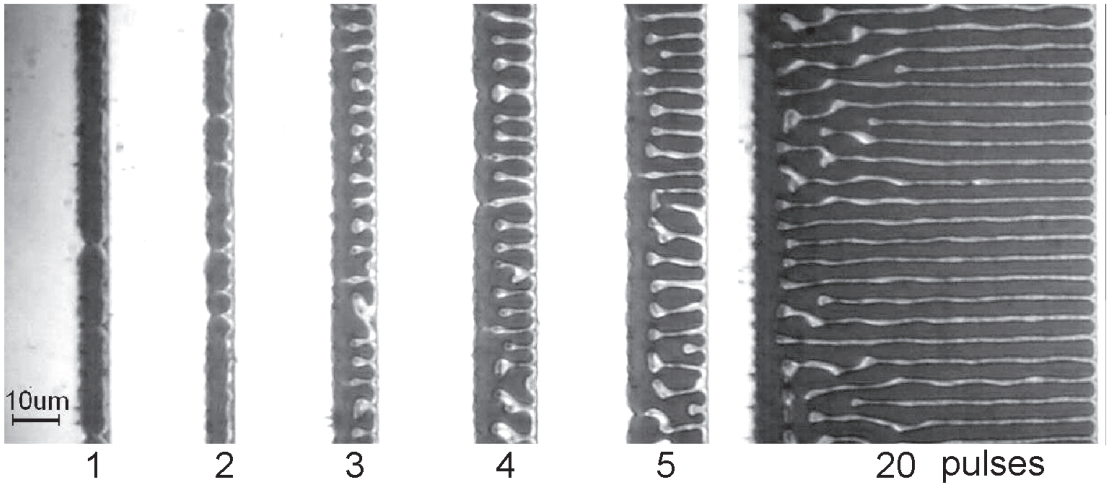

Fig. 22 Initial stage of ripple formation in the Cr film on glass. Numbers below (N = 1, 2, 3, 4, 5, 20) indicate the number of laser pulses with the shift between them of Δx = 0.4 μm applied to remove the metal in the stripe. Laser fluence F_0 = 2.04 J·cm^{-2}, laser spot was 2.5 mm × 2.5 μm oriented vertically.

The starting point of the ripple line looked like a droplet of the solidified metal. The surface tension of liquid metal forced collection of the metal in an energetically more favorable shape. Local dewetting of the substrate took place when laser fluence was not able to evaporate the whole thickness of the film.

The irradiation of the Cr film with further laser pulses, keeping the same shift between them, stabilized the period and shape of the ripples. Perturbation in the laser beam distribution or the film thickness caused defects in regular ripples, but they were healed by applying another 3-5 shifted pulses. The ripples were formed when laser fluence was above the threshold of the film removal with a single pulse. Because of ridges on the sides of the cleaned area, higher energy density was required for complete removal of the metal. Three times higher fluence was only able to clean the substrate completely.

4.2.5 Process window for the ripple formation

The period of the ripples depended on the laser pulse energy and the overlap. In order to find out the ripple formation window, the laser pulse energy and spacing between overlapping pulses (shift) were varied, and morphology of

changes in the chromium film was investigated by optical microscopy. Typical shapes of patterns formed of the 100 nm-thick chromium film by laser radiation depending on the laser fluence and the beam overlap are presented in Fig. 23.

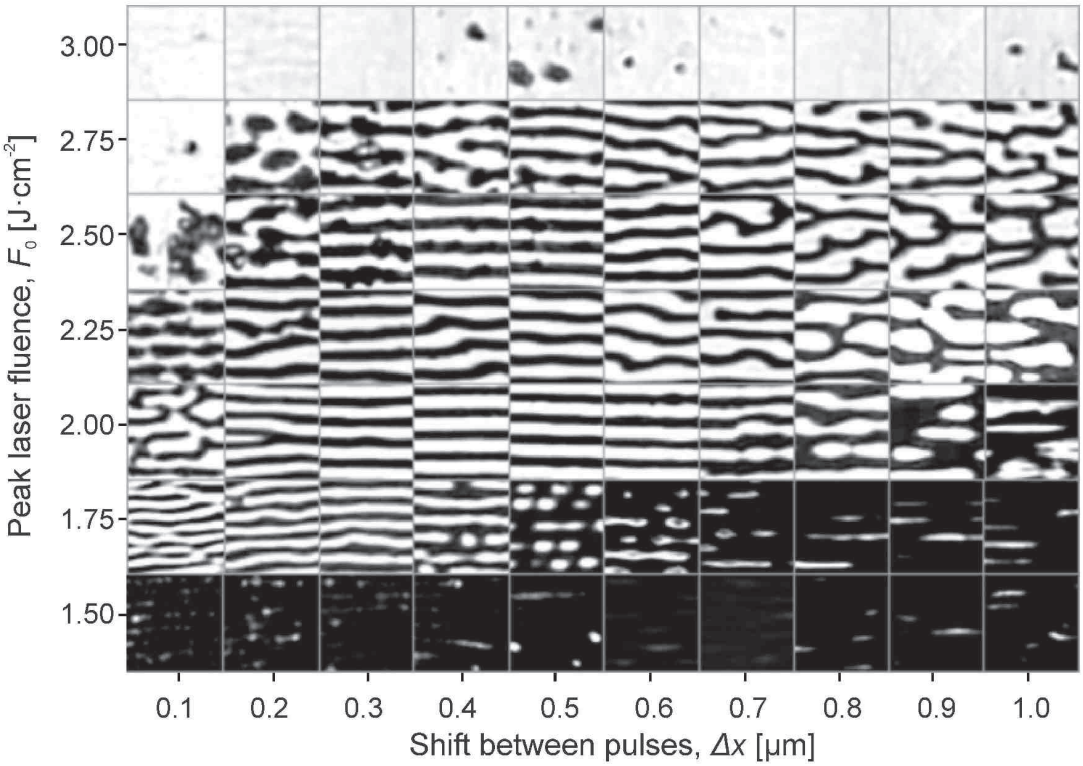

Fig. 23 Optical transmission microscope photographs of the pattern formed in the laser irradiated, 100 nm thick chromium films on the glass substrate depending on the laser fluence and the beam overlap (shift). Actual size of each picture is 19.5 μm × 19.5 μm.

The remaining chromium is not transparent leaving the black colored areas in pictures, while white color corresponds to the areas where the metal was removed completely. The shift direction of laser pulses with respect to the sample in all pictures was from the left to the right. The best conditions for the perfect ripple formation were at the fluence in the range of 1.7 – 3.0 J·cm^{-2} and the shift of the overlapping pulses from 0.3 to 0.4 μm. For the shift less than 0.2 μm or more than 0.6 μm, the ripples became irregularly shaped. When the

laser fluence was further increased to 3.0 J·cm^{-2}, the ripples disappeared completely and clean removal of a wide stripe of the metal film was achieved.

The effect of ripple formation was not sensitive to the initial thickness of the chromium film (see Table 6).

Table 6 Formation of regular gratings in the chromium films of different thickness depending on processing parameters.

Film thickness, h [nm]	Peak laser fluence, F_0 [J·cm^{-2}]	Shift between pulses, Δx [μm]	Grating period, Λ [μm]
190			irregular
150	1.6-2.1	0.2–0.6	3.6
120	1.4-2.1	0.1–0.8	4.0
100	1.7-2.7	0.1–0.9	4.4
80	1.1-2.1	0.1–0.5	3.6
50–60			irregular
35–40			irregular

The morphological features (cracking, melting and ripple formation) were almost the same for the case of the 120 nm, 150 nm and 190 nm thick chromium films, as those of the 100 nm chromium film. However, the formation of regular ripples with straight lines was not achieved in the case of the 60 nm-thick chromium film.

4.2.6 Reconstruction of ripples after a defect

Stability of the ripple formation process was tested with initially defected Cr films (holes were ablated with a spherically focused laser beam). Reconstruction of the former regular ripple structure occurred after irradiation with the same 3–5 further laser pulses at a short distance passing the defect (Fig. 24).

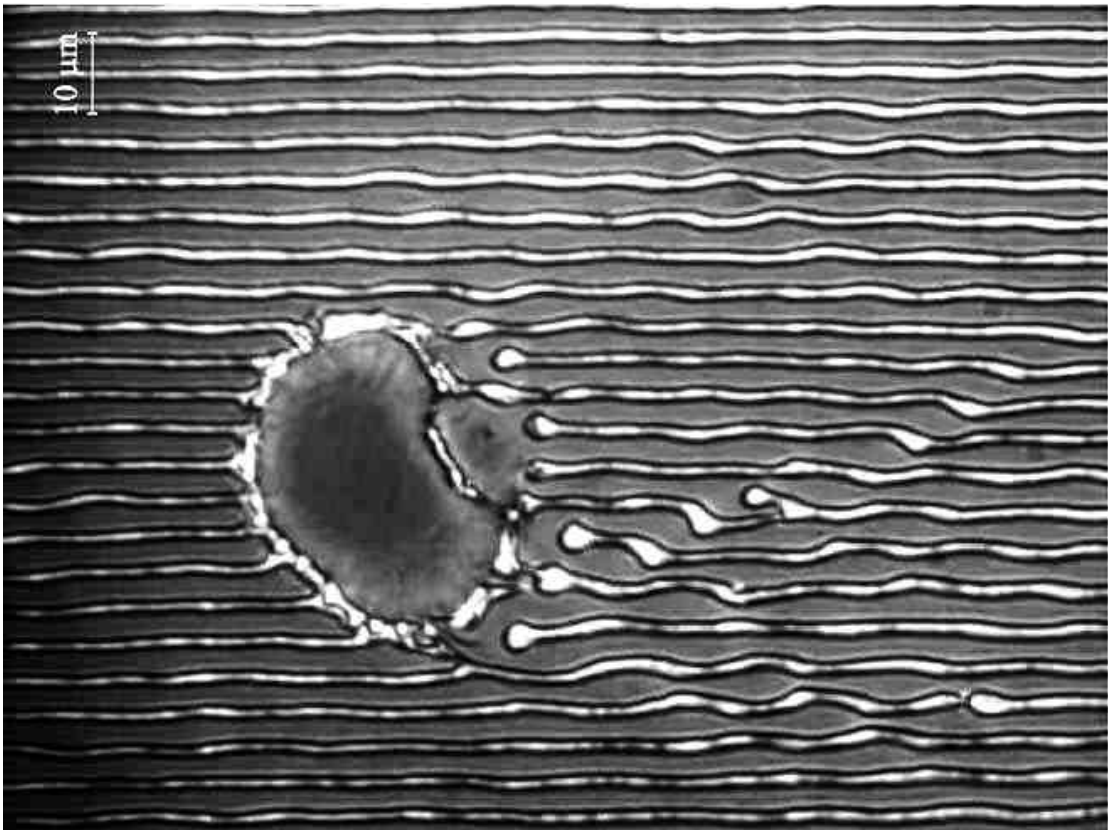

Fig. 24 Healing of the ripple structure after passing the defected area (cleaned by a circular laser spot). The scanning direction was from the left to the right.

Perturbations in laser intensity distribution or the film thickness caused the coalescence or evanescence of the ripple lines. No splitting of the ripple line in two lines was observed.

4.2.7 Crack propagation in metal film

One of stabilizing factors in the ripple formation could be cracks in the thin Cr film and the glass substrate propagating behind the laser irradiation area. The cracks were found by investigation of the samples with SEM (Fig. 25).

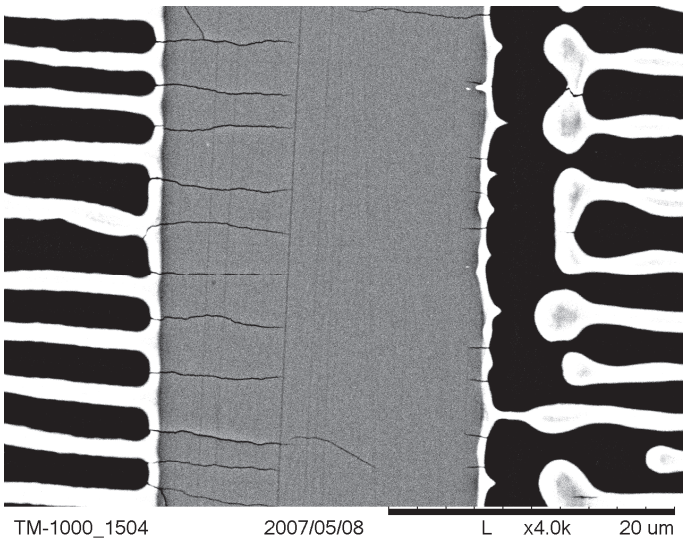

Fig. 25 SEM image of ripples formed of the thin chromium film with partially overlapped laser pulses. Shift between pulses $\Delta x = 0.3$ μm (left) and $\Delta x = 0.4$ μm (right), laser fluence $F_0 = 1.8$ J·cm^{-2}.

The picture shows an area between two experiments with the shift between laser pulses of 0.3 μm and 0.4 μm. The ablation area was as broad as 50 μm in both experiments and only the finishing part on the left and the initial part on the right of the experiments are shown in the picture. The central part in the picture was not irradiated with the laser. Cracks on the initial part (right) are short because they were formed from the very first pulse in the sequence. The cracks on the finishing part (left) propagated as deep as 10 μm into the non-irradiated area, as prolongation of the ripples. However, the cracks were more irregular than the ripples. Cracking of the film was caused by the thermal expansion mismatch of the thin film and the substrate.

4.3 CONCLUSIONS

Overlapping laser pulses initiated self-organization in chromium thin film on glass when laser fluences exceeded the single pulse ablation (removal) threshold. Formation of regular structures, ripples, at laser ablation of the thin chromium film has been shown. The ripples were located periodically ($\Lambda \approx 4$ μm) parallelly to the laser pulse shift direction.

5 FABRICATION OF PERIODICAL GRATINGS

Material related to this chapter was published in [A2], [A5] and [C7], [C8], [C9].

Because regular structures were produced, attention was paid to their possible application. The new method of diffraction grating fabrication in thin metal films on a glass substrate was developed and verified. Further experiments were conducted in order to characterize the gratings and investigate possibilities of controling their period.

5.1 PERIODICAL GRATING FABRICATION

Formation of the highly regular gratings of ripples was observed in a certain range of laser fluences and beam overlap. When the laser fluence was above the threshold and the shift between pulses was less than half the width of the line ablated with a single laser pulse, regular ripples were developed. The most regular ripples, periodical gratings, were formed when the laser fluence was 30% above the ablation threshold (see Fig. 26).

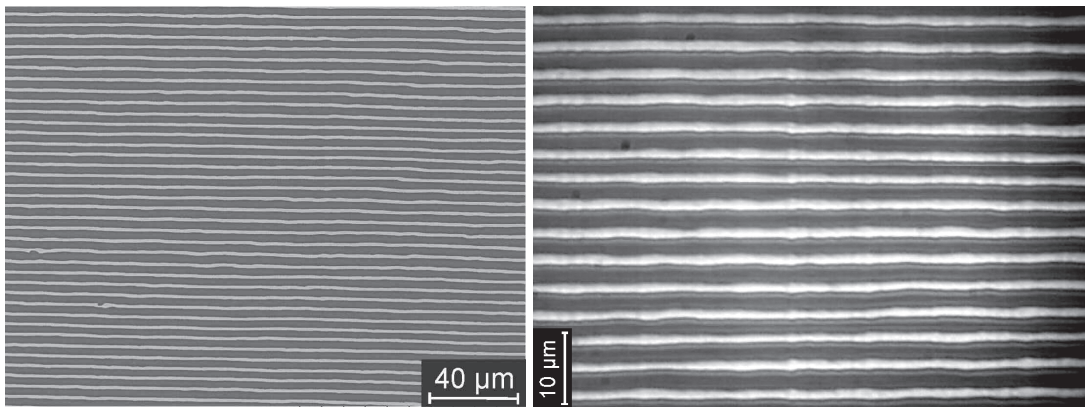

a) b)

Fig. 26 Cr grating on the glass substrate made by self-organization under the nanosecond laser irradiation. (a) SEM image: laser fluence $F_0 = 2.0$ J·cm^{-2}, shift between laser pulses $\Delta x = 0.6$ µm, (b) optical microscope image: $F_0 = 1.9$ J·cm^{-2}, $\Delta x = 0.3$ µm.

The periodical ripple grating of the unlimited length can be formed using this method. Experimentally, the grating of ripples was formed with the 1 cm length and straight lines without any defects.

5.2 CHARACTERIZATION OF GRATINGS

The quality of the self-organized gratings was evaluated. For this purpose, the laser beam of a small diameter passed through the grating and diffraction patterns were captured by the CCD camera (see Fig. 17). The diffraction patterns were measured by illumination of the grating at various distances y from the center of the grating. The scanning direction y corresponded to the long axis of the laser spot. Positions of diffraction pattern (angle φ) are related to the grating period Λ, the order of diffraction maximum m and the laser wavelength λ (633 nm in our case) by equation [166]:

$$\Lambda \sin\varphi = m\lambda, \tag{52}$$

where φ is the diffraction angle, m is the integer number. The zero, first and second order diffraction patterns (m = 0, ±1, ±2) are given in Fig. 27.

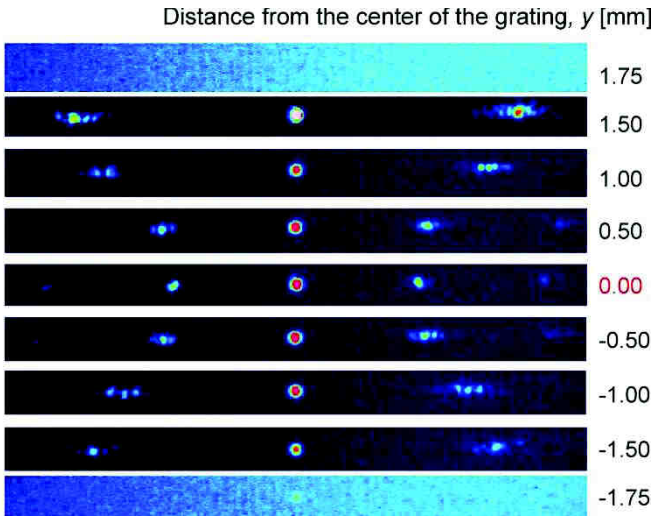

Fig. 27 Diffraction patterns at various distances from the grating center measured by the CCD camera and the HeNe-laser illumination.

5.3 CONTROLLING THE GRATING PERIOD

The central image (coordinates 0.00) corresponds to the center of the grating where the grating was highly periodic and its period was the largest, nearly $\Lambda = 4$ μm, corresponding to the smallest diffraction angle. The shapes of maxima were round and narrow. As the laser spot used to form the gratings by laser ablation was elliptical with the high aspect ratio, the central part of the grating (in y direction) was prepared at the highest laser intensity. Moving from the center, the intensity fell down and the grating lines were closer to each other. The period Λ of 2.4 μm was estimated from diffraction patterns on periphery of the laser irradiated area ($y = \pm 1.5$ mm). The laser spot dimension in this direction was 2.5 mm (e^{-2} level). At the distance $y = \pm 1.75$ mm from the center of the grating no diffraction maxima were seen because the grating was not formed there. The measured grating period versus the distance from the center is plotted in Fig. 28:

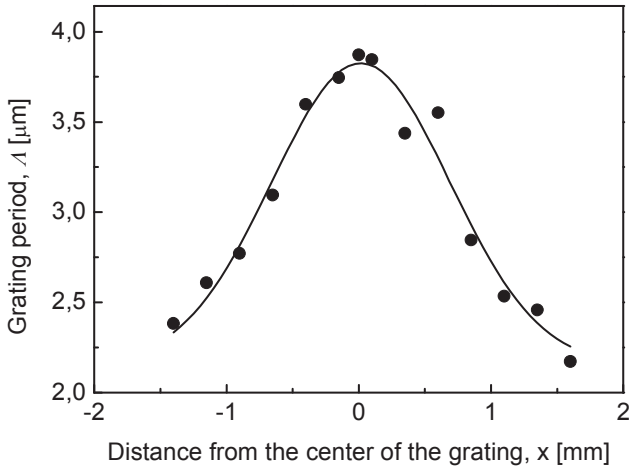

Fig. 28 The grating period versus distance from the grating center. Dots correspond to experimental data and the solid line is the Gaussian fit.

The period of the grating formed by self-organization of the metal film varied together with the Gaussian profile of the laser spot. Out of the center, conditions for the regular grating formation were not optimal, leading to

modulation in the grating period. Evidence to that was splitting of the first order diffraction maximum due to the grating aperiodicity (see Fig. 27).

5.3.1 Grating period vs laser fluence

Because the grating period varied by the Gaussian law as a function of the distance from the center (see Fig. 28), and the same distribution was valid for the laser intensity given by Eq. (50), it is obvious that the grating period is linearly proportional to the laser energy density. The grating period versus laser fluence is plotted in Fig. 29.

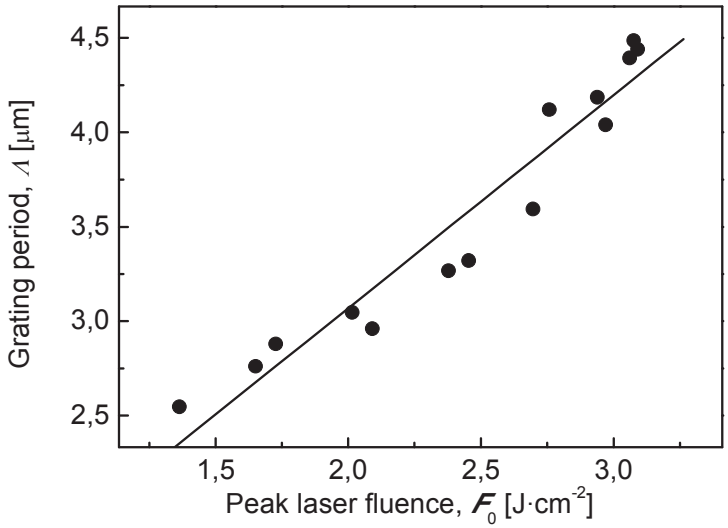

Fig. 29 Grating period as a function of peak laser fluence. Dots correspond to experimental data and solid line is a linear fit of the data points.

The ripples in gratings were formed of the melted metal which remained after the film ablation. The higher the intensity, the more metal was evaporated. Formation of the stable ripple line in the grating required a certain amount of chromium to melt. As less metal was left in the center because of higher intensity of the laser radiation, dewetting and surface tension forces collected the melt from a broader area, increasing the period. The evidence of that was variation in the grating period with a shift between laser pulses.

5.3.2 Grating period vs shift between pulses

In order to find out more process parameters which can control the grating period, additional experiments were performed by varying spatial separation between consecutive partially overlapping laser pulses. The grating period as a function of the shift between laser pulses is shown in Fig. 30.

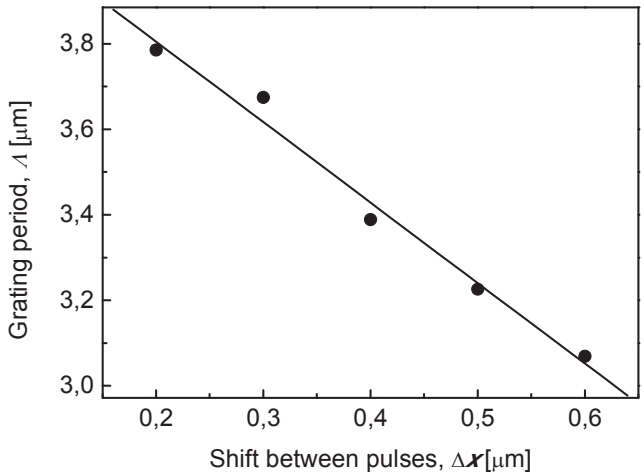

Fig. 30 Grating period as a function of shift between laser pulses. Dots correspond to experimental data and solid line is a linear fit of the data points.

The grating period decreased linearly with an increase in the distance between the laser pulses. A smaller shift between laser pulses meant the larger overlap. The irradiation dose to the metal film was higher in this case, less metal remained after irradiation and more detached lines were formed. The results show that the period of the gratings formed by self-organization can be controlled by changing the laser fluence or the shift between laser pulses.

5.4 CONCLUSIONS

The ripples were located periodically parallel to the laser pulse shift direction. The period can be varied from 2.5 to 4 μm. The period of ripples increases linearly by increasing the laser pulse fluence and decreases linearly by increasing the shift between pulses.

Diffraction gratings can be manufactured by the laser induced self-organization. The uneven intensity distribution on the long axis of the strip-like spot caused variation in the grating period and the outspread of the first diffraction maximum. The top-hat intensity distribution on the long axis of the strip-like spot should be applied to produce good quality gratings with the vanishing period variation.

6 CASE OF OTHER METALS: LASER IRRADIATION OF ALUMINUM, COPPER, GOLD AND SILVER FILMS

Material related to this chapter was published in [A1] and [C4].

Different types of metals were used in experiments in order to understand the reasons for the regular structure formation in the chromium film. In all cases the minimal laser fluence which was able to completely ablate the metal film trough the whole its depth was estimated. When a single laser pulse with the fluence higher than this ablation threshold specific to the particular metal was applied, the linear trench was ablated in all the films. The laser fluence was kept above it in the range of 1.5-3 F_{th} during the experiments. A diverse behavior of the films under laser irradiation was observed depending on the metal when a burst of partially overlapping pulses was applied.

6.1 NO RIPPLES IN ALUMINUM FILM

The thin aluminum film was completely removed by laser ablation with overlapping laser pulses when the laser fluence exceeded the ablation threshold.

6.2 DEWETTING IN THIN COPPER FILM

The next coming laser pulses were also not capable of evaporating the whole film in case of copper similar to the thin chromium film. A lot of holes opened along the laser spot in the film irradiated with overlapping pulses. The holes were assembled into complicated structures but we did not find any regime for regular self-assembly of the laser irradiated copper film on glass (Fig. 31).

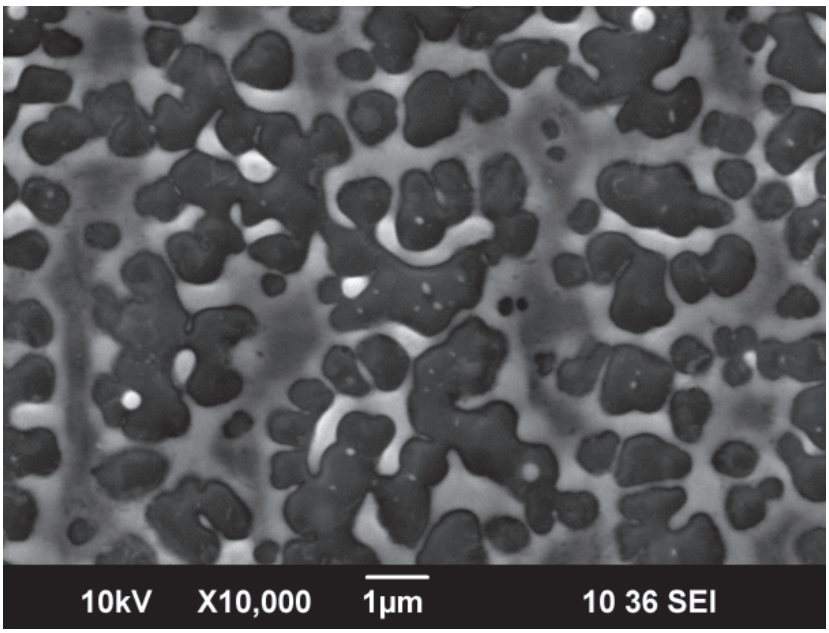

Fig. 31 SEM image of Cu film processed with the overlapping laser pulses. Bright areas are covered with remaining copper. Laser fluence $F_0 = 4.2$ J·cm^{-2}, shift between pulses $\Delta x = 0.05$ µm. The laser spot is oriented vertically. Shift of the laser pulses from the left to the right side of the sample.

Regular structures did not appear in thin Cu metal film on a glass substrate. Particles with the mean size in the range of 700 - 900 nm were formed attached to a glass substrate.

6.3 THREE KINDS OF RIPPLES IN THIN GOLD FILM

In gold, three kinds of regular structures were found after laser irradiation with a sequence of partially overlapping laser pulses: longitudinal (similar to ripples in chromium), transverse and a structure of inclined ripple lines (see Fig. 32).

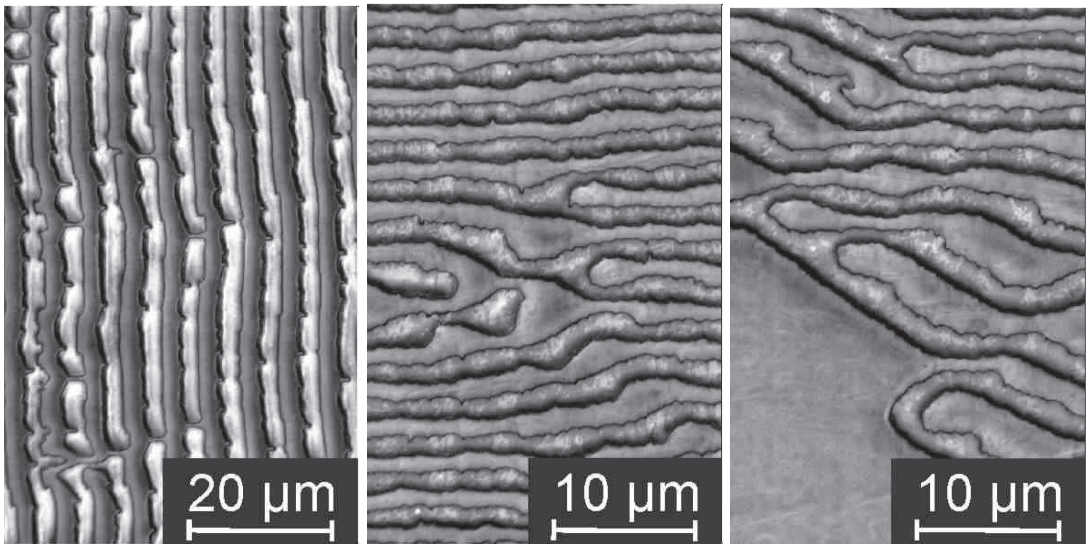

a) b) c)

Fig. 32 SEM images of thin Au film processed with overlapping laser pulses in areas of the transversal (a), longitudinal (b) and inclined (c) ripple formation: openings of diverse shape were formed in the gold film. The linear spot in the pictures was oriented vertically and scanned from left to right at various shifts between pulses (overlaps) and laser fluences: a) laser fluence $F_0 = 4.51$ J·cm^{-2}, shift between pulses $\Delta x = 60$ nm, period of ripples $\Lambda = 6.5$ µm; b) $F_0 = 4.71$ J·cm^{-2}, $\Delta x = 25$ nm, $\Lambda = 3.5$ µm; c) $F_0 = 4.85$ J·cm^{-2}, $\Delta x = 10$ nm, $\Lambda = 5.2$ µm.

At lower fluences, the ridges formed after the film ablation prevented removal of the film until the shifted laser spot reached an area of the film with the initial thickness (Fig. 33).

The period was nearly independent of the shift between pulses and it was in the range of 5.6-7.1 µm. The width of the laser cleaned area in the shift direction was around 3 µm, and the ripple line was also about 3 µm in width. The transversal structure was not stable and was not related to the self-organization in the molten metal film.

Moderate fluences and small shift between pulses resulted in the "Christmas tree" type structure development after irradiation with numerous laser pulses (>50). They appeared with some delay (shift) from the zone ablated with the first laser pulse in a burst. Linear openings appeared in the metal film, and their direction was different from those of the laser spot or the

sample shift. The angle between the linear cleaned areas was 57-63 degrees. The effect was observed in a close range of laser fluences of 4.5-5.0 $J \cdot cm^{-2}$ when the shift between pulses was in the range of 5-20 nm (the number of laser pulses per area $N > 100$). The period of the ripples was about 5 μm.

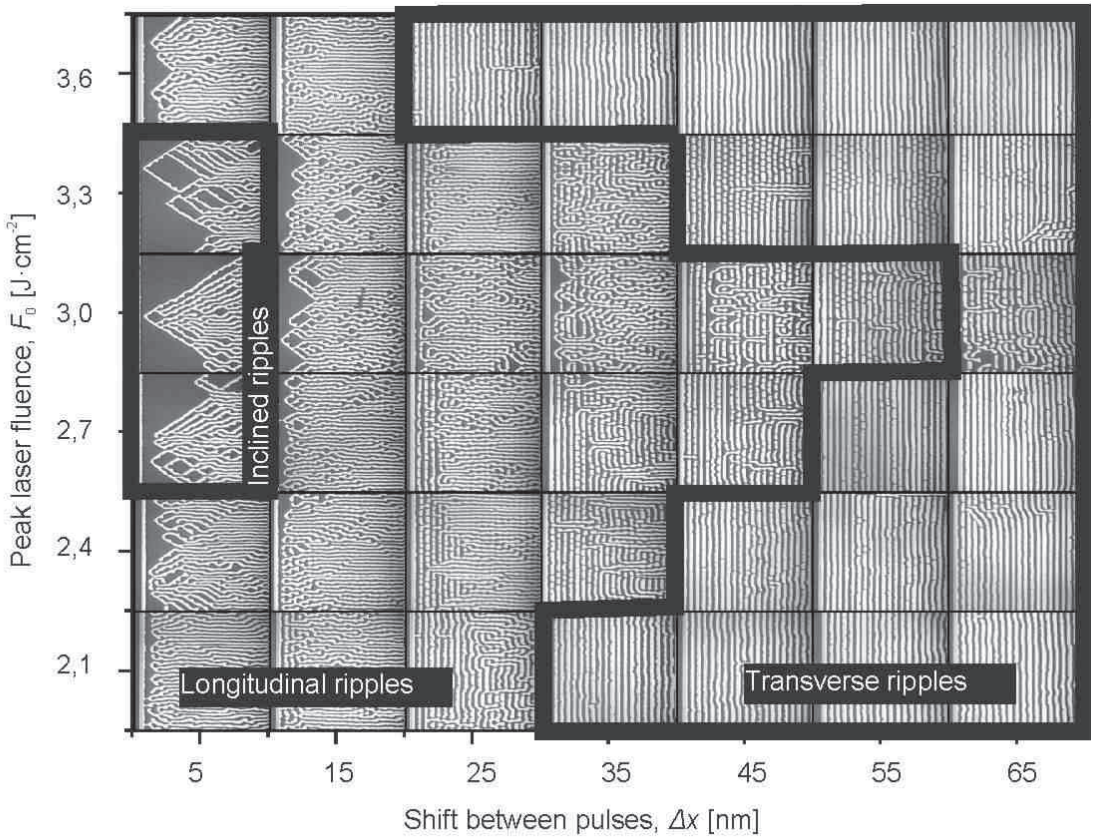

Fig. 33 SEM image of ripples in thin gold film at various laser fluences and shift between pulses. Note inclined (left), longitudinal (middle) and transversal (right) ripples at different laser processing regimes. Actual size of each picture is 120 μm × 120 μm.

Ripples of this kind were competing with formation of longitudinal (parallel to the shift direction) ripples, similar to those observed in chromium films. The period of the longitudinal ripples was 3.1-3.5 μm with characteristic bifurcation (Fig. 32b). This kind of self-organization was observed at the same laser fluences but in a wider range of the shift between laser pulses.

As the lattice of gold is a face-centered cubic, the angle of 60 degrees indicates that the film was solidified in a crystallographic plane (111).

Dislocations initiated formation of openings in the film with specific orientation of ripples with a preferable angle of 60 degrees between them.

6.4 DELAMINATION OF SILVER FILM

The first pulse in the burst ablated silver from the glass substrate. The effect of following laser pulses was completely different in comparison with other metals (see Fig. 34).

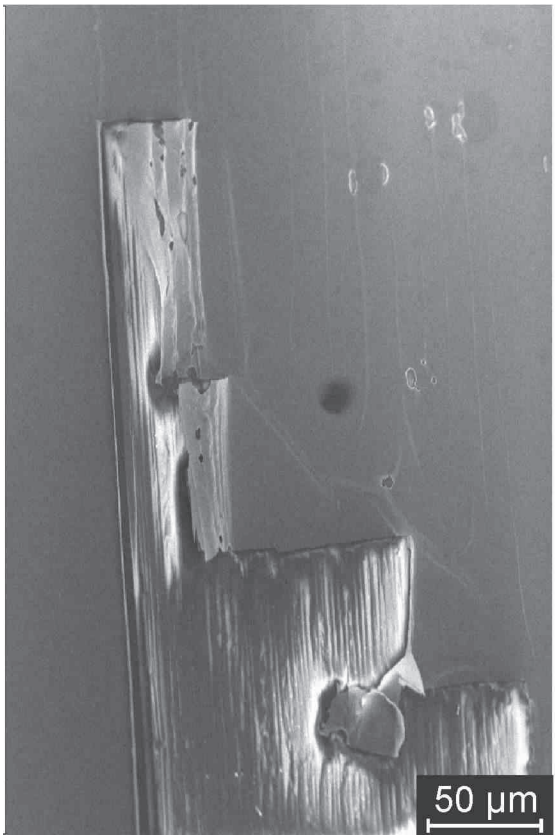

Fig. 34 Image of ablated thin silver film with the overlapping laser pulses.

The silver thin film had bad adhesion to the substrate. It delaminated from the substrate after the irradiation with laser pulses due to the vapor pressure and low adhesion at the glass - metal interface.

6.5 CONCLUSIONS

A diverse behavior of metal films on glass was observed after irradiation with a sequence of partially overlapping laser pulses when the energy density was above the single-pulse ablation threshold. Regular longitudinal ripples were specific to the chromium film and also to gold in a very narrow window of the process parameters. Laser radiation did not transform the initial array of holes in the copper film into a regular structure.

7 MODEL OF RIPPLE FORMATION IN THIN CHROMIUM FILM UNDER NANOSECOND LASER IRRADIATION

Material related to this chapter was published in [A1] and [C1], [C3], [C4], [C5].

In this chapter the experimental data are compared with simulations based on different physical phenomena in order to develop and confirm a model of ripple formation in the thin chromium film under its irradiation with pulses of a nanosecond laser.

7.1 MODEL OF PERIODICAL CHROMIUM FRACTURE

The first model was developed based on an apparent fact that the chromium film fractures when it is heated with a laser beam (see Fig. 25), and it can be divided into four steps.

1. The chromium thin film and the glass substrate underneath fracture because of the thermal expansion mismatch [167];
2. Cracks propagate ahead of the laser irradiation area;
3. The next slightly shifted pulse melts chromium;
4. The molten chromium between two cracks tends to decrease its surface energy by assembly into a wire-like ripple due to surface tension.

Cracks normally originate perpendicular to the long extent of the laser spot and parallel to the shift direction. For a thin chromium film heated by the laser irradiation, the buckle delamination coefficient was estimated from Eq. (18) and for chromium and glass parameters from Table 1 and Table 4. The buckling and fracture period was found to be equal to $\Lambda = 3.8\,\mu\text{m}$ for our experimental conditions. The buckling and fracture period agrees well with the chromium fracture period in the experiments and is close to the ripple period. However, during detailed investigations of cracks in the Cr film in SEM

pictures similar to Fig. 25, it was evident that the cracks were more unstable than the regular ripples. Splitting of the ripple line into two ones was never observed, while the metal between a few cracks was assembled into a single ripple line.

Even that the period of cracks in the chromium film caused by a buckling is close to the ripple period, the effect is not capable of stabilizing the process of a regular ripple formation in the laser-heated film.

7.2 MODEL OF RIPPLE FORMATION

The model of ripple formation was prepared based on experimental data and the process can be divided into six stages:

1. A laser beam with the Gaussian distribution in x direction is applied to remove the thin chromium film from the glass substrate in the back-side irradiation geometry (Fig. 35a).
2. A single pulse removes (evaporates) chromium from glass in an area with the width of D_x (Fig. 35b).
3. Ridge is formed on a rim of the ablated area because of the thermo-capillarity effect (Fig. 35c).
4. The Plateau-Rayleigh instability modulates the ridges into a droplet-like structure with the characteristic wavelength Λ (period between droplets) (Fig. 35d).
5. The second shifted pulse melts the ridge and Marangoni (thermo-capillarity) forces move the melt in x direction because of the temperature gradient forming a ridge in a new position in x direction (Fig. 35e).
6. The next shifted pulse, uniform in y direction, melts the ridge and the temperature modulation in y direction occurs due to the heat dissipation to the ripples starting to grow from the initial droplets. The Marangoni convection pushes the metal from the hotter area in the ridge to the cooler ripples (Fig. 35f).

The following sections of this chapter are dedicated to simulation of the effects involved in the ripple formation and estimation of parameters which are responsible for the period of regular ripples.

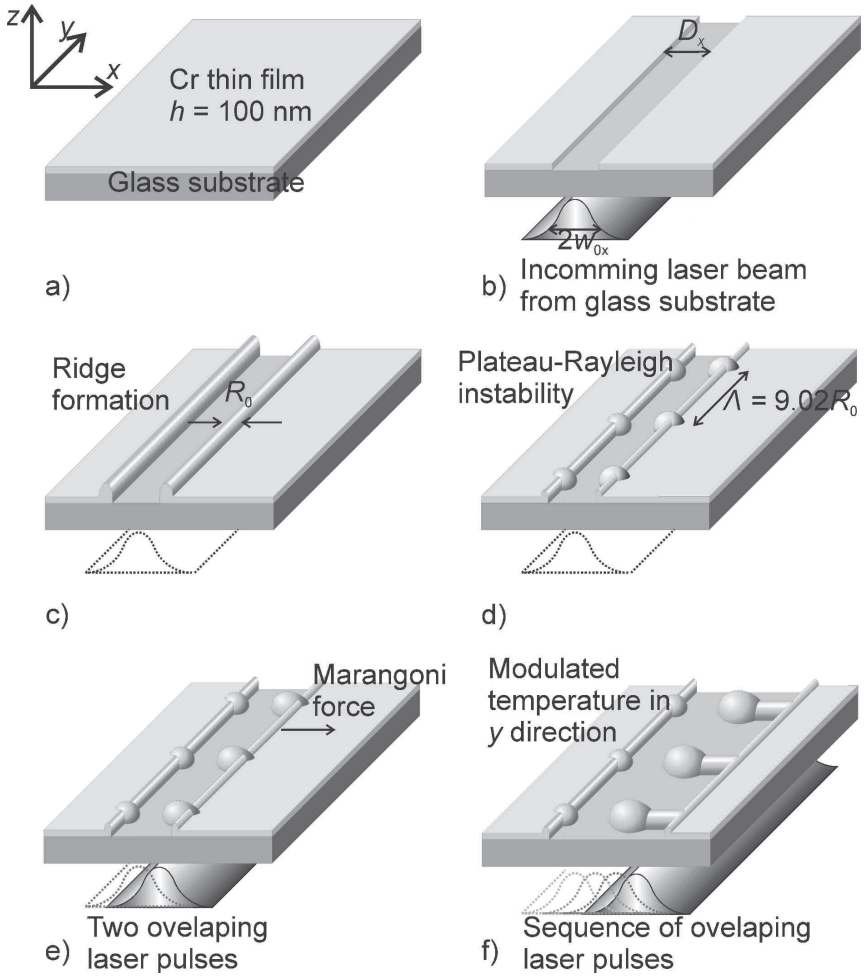

Fig. 35 Stages of ripple formation: (a) thin chromium film on a glass substrate, *xyz* denotes spatial coordinates; (b) the linearly focused laser beam width of $2w_{0x}$ irradiates from the bottom. A laser pulse ablates the line with a width of D_x; (c) the cylindrical ridge with a width of R_0 is formed; (d) the cylindrical ridge transforms into droplets with the periodicity of Λ because of the Plateau-Rayleigh instability; (e) the second shifted laser pulse re-melts the ridge and Marangoni forces move the ridge towards right; (f) every next pulse re-melts the ridge which is shifted due to the Marangoni force and the liquid metal is redistributed into regular ripples.

7.2.1 Ridge formation and Plateau-Rayleigh instability

Ridges of the resolidified metal were always formed on edges of the ablated area (Fig. 18a). The profile of the ridges was measured with AFM. The metal layer in ridges was as high as 400 nm while the original Cr film was only 100 nm thick. The thickness of chromium in ridges increased up to four times in comparison to the initial thickness of un-irradiated thin chromium film. The thicker chromium layer in the ridge could not be removed with the same laser fluence because the ablation threshold is linearly proportional to the thickness of the films [152, 154].

The ridges were not uniform in their thickness along the rim of the laser ablated area. Droplet-like structures can be recognized by AFM and SEM techniques. Analysis of the pictures led to the conclusion that the Plateau-Rayleigh instability forced the metal in the ridges to form periodical droplets with the predictable periodicity Λ described by Eq. (8).

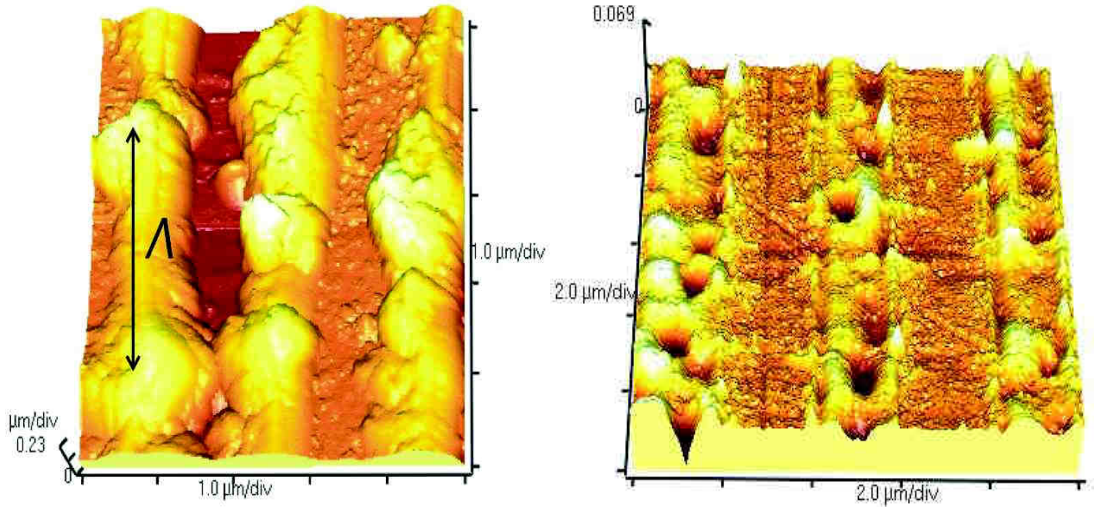

a) b)

Fig. 36 3D AFM pictures of areas ablated with a single laser pulse: a) ablated area with ridges on both sides, Λ denotes the distance between two droplets formed off a ridge due the Plateau-Rayleigh instability (F_0 = 1.9 J·cm^{-2}); b) the Cr film irradiated from the backside with three not-overlapping laser pulses with a linear shaped spot and fluence close to the threshold (F_0 = 1.45 J·cm^{-2}). Note that holes and droplet-like ridges are distributed nearly periodically.

Close to the threshold, holes appeared in the metal film, instead of the complete film removal in the irradiated area (Fig. 18b). The holes were surrounded by ridges of the recast metal. As the backside illumination was used, holes were formed by a vapor eruption from beneath (inner interface). The holes were aligned along the linear spot with quasi-periodical distribution. The resolidified ridge width and the Plateau-Rayleigh modulation periodicity versus peak laser fluence in the pulse from SEM images are given in Fig. 37.

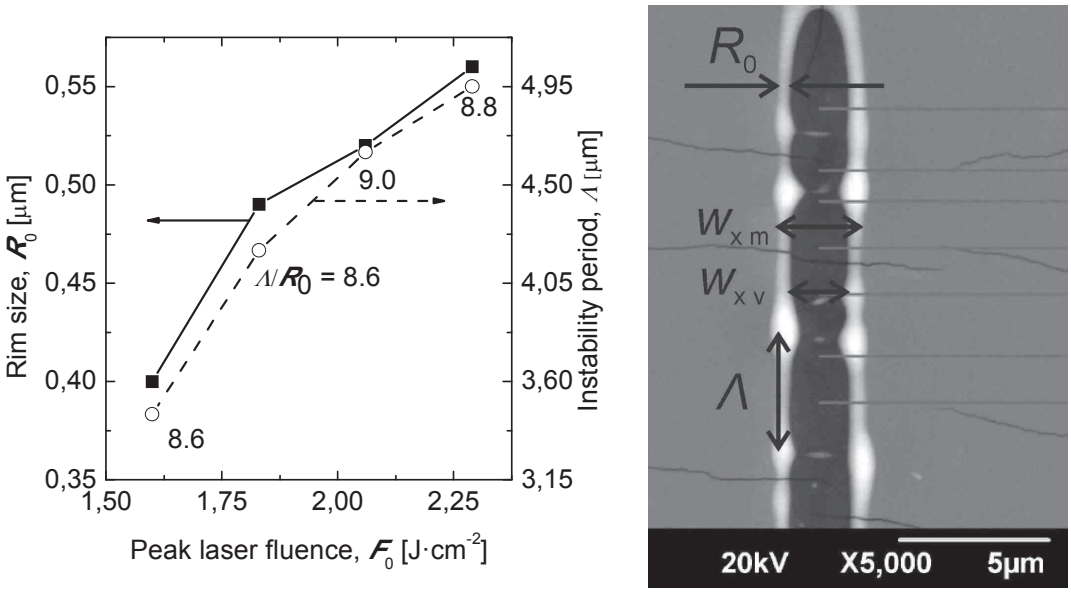

a) b)

Fig. 37 (a) Ridge size and instability period versus peak laser fluence. The numbers below the points indicate the ratio between the ripple period and the rim width (radius) corresponding to Eq. (8); (b) SEM image of Plateau-Rayleigh instability in the chromium ridge after a single-pulse laser ablation (F_0 = 1.8 J·cm^{-2}), Λ indicates the wavelength of instability and R_0 is the ridge size. Again, cracks are less regular than droplets.

The average ratio of the instability period to the radius of the resolidified ridge was close to 9.02 and this is a clear evidence of the Plateau-Rayleigh instability because the mode with a ratio of 9.02 between the period and the

radius is dominant (grows in the fastest way). The mechanism of ridge formation at different laser fluences is schematically shown in Fig. 38.

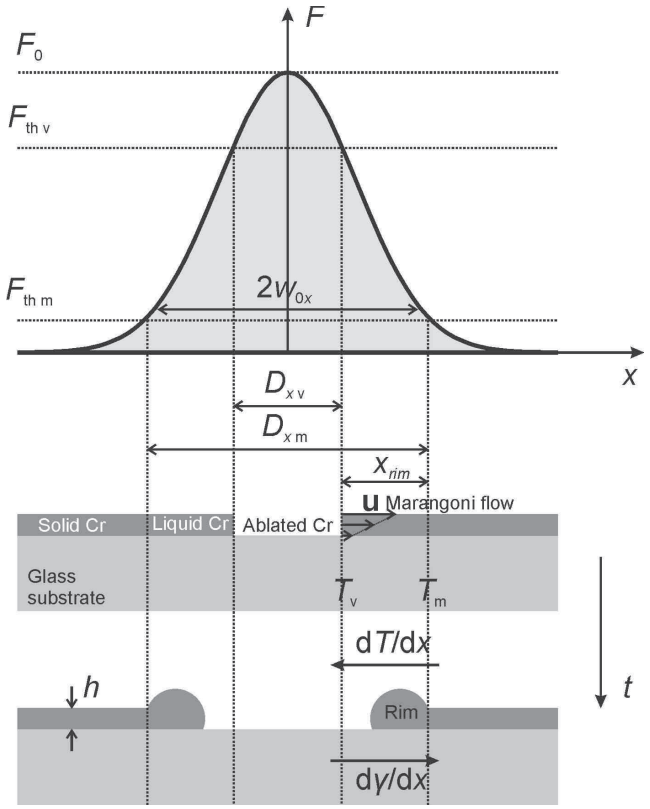

Fig. 38 Ridge formation scheme. The Gaussian beam applied to thin chromium film, F is the laser fluence, F_0 is the peak laser intensity, $F_{\text{th v}}$ is the vaporization threshold, $F_{\text{th m}}$ is the melting threshold, $2w_{0x}$ is the beam diameter in x direction, $D_{x\,\text{v}}$ is the width of evaporated chromium, $D_{x\,\text{m}}$ is the full width of melded chromium, x_{rim} is the width of melted chromium on a rim, h is the thickness of thin chromium film, **u** is the Marangoni flow velocity due to the temperature gradient dT/dx in molten chromium, dγ/dx is the surface tension gradient in molten chromium, t is a time.

The theoretical threshold for melting and evaporation of the thin chromium film was computed using Eqs. (44) and (45) and the chromium parameters from Table 1. The room temperature $T_0 = 293$ K, the peak laser fluence $F_0 = 2.0\ \text{J}\cdot\text{cm}^{-2}$, the focused beam radius $w_{\text{x0}} = 2.5$ μm. The computed melting and evaporation thresholds were $F_{\text{th m}} = 0.22\ \text{J}\cdot\text{cm}^{-2}$ and $F_{\text{th v}} = 1.41\ \text{J}\cdot\text{cm}^{-2}$, respectively. The full widths of melted and evaporated areas in x direction

found from Eq. (42) are equal to $D_m = 5.3\,\mu m$ and $D_v = 2.1\,\mu m$. The width of molten chromium on a rim can be estimated as $x_{rim} = (D_m - D_v)/2 = 1.6\,\mu m$. Having the width of molten chromium, an approximate radius of a ridge can be estimated from the mass conservation of molten metal and the value was equal to $R_0 \approx \sqrt{x_{rim} h} = 0.4\,\mu m$. The value is in agreement with that we obtained from AFM measurements. This provides the Plateau-Rayleigh instability period from Eq. (8) $\Lambda = 3.6\,\mu m$ and the characteristic instability growth time by Eq. (9) $\tau_0 = 44$ ns. The computed period of the Plateau-Rayleigh instability in the ridge formation and the growth time correspond well to the experimentally measured period and the time period when liquid chromium exists. This was a clear evidence that the Plateau-Rayleigh instability initiated the begging of ripple formation.

The ridge formation was metal dependent. Large ridges were formed only in the thin chromium film as shown in Fig. 39.

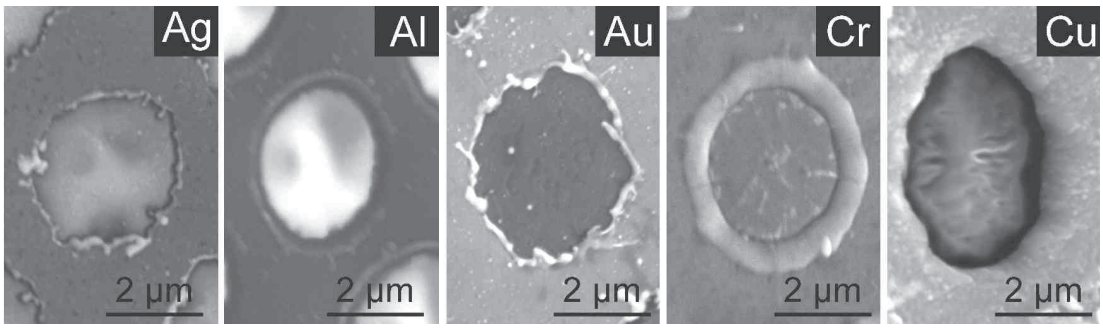

Fig. 39 SEM images of the holes ablated in metal films by the rare-side laser ablation. Note differences in ridge formation in various metal films on the glass substrate.

The largest ridge size was formed in thin Cr film because of the strongest film adhesion to the glass substrate (see Table 3). This prevented the thin chromium film from delamination off the substrate when heated to the melting point. Other materials such as Ag, Al, Au and Cu had lower adhesion to the glass substrate (see Table 3). Therefore, delamination took place when heated to the melting point. A small ridge was formed, and its size is crucial for the Plateau-

Rayleigh instability periodicity. This explains why regular ripples were formed only in the thin chromium film.

Marangoni force which drives molten metal from hot to cold areas plays an important role in the ridge formation. The strength of the effect is described by Marangoni number from Eq. (6) given in Table 7.

Table 7 Marangoni numbers of metals calculated by Eq. (6) and data from Table 3.

Metal	Marangoni coefficient, Ma [a.u.]
Ag	35
Al	105
Au	33
Cr	117
Cu	58

Chromium again has the largest Marangoni coefficient among investigated metals. A high value of the Marangoni coefficient in combination with the strong adhesion to the glass substrate makes the ridge formation possible and the Plateau-Rayleigh instability initiates the first stage of the regular ripple formation.

7.2.2 Steady growth of regular ripples

Profile of the ripples was measured with AFM. The volume of the metal was estimated from the ripple line shape and it was compared with the volume of the untreated metal in the film. In case of chromium, the volume of metal remaining in ripples was 90-110% of the initial metal volume. The AFM microscopy showed that almost all chromium remained on the glass substrate, and only a small portion of the metal was ablated. This means that under experimental conditions of regular ripple formation in the chromium film no significant evaporation occurred (higher than 100% value means that voids

were present in the metal of ridges). Laser irradiation stimulated redistribution of the molten metal on a substrate.

The regular ripple formation was a stationary process because every next laser pulse produced the same end of "the end of the ripples" elongated by the laser pulse shift Δx (see Fig. 40).

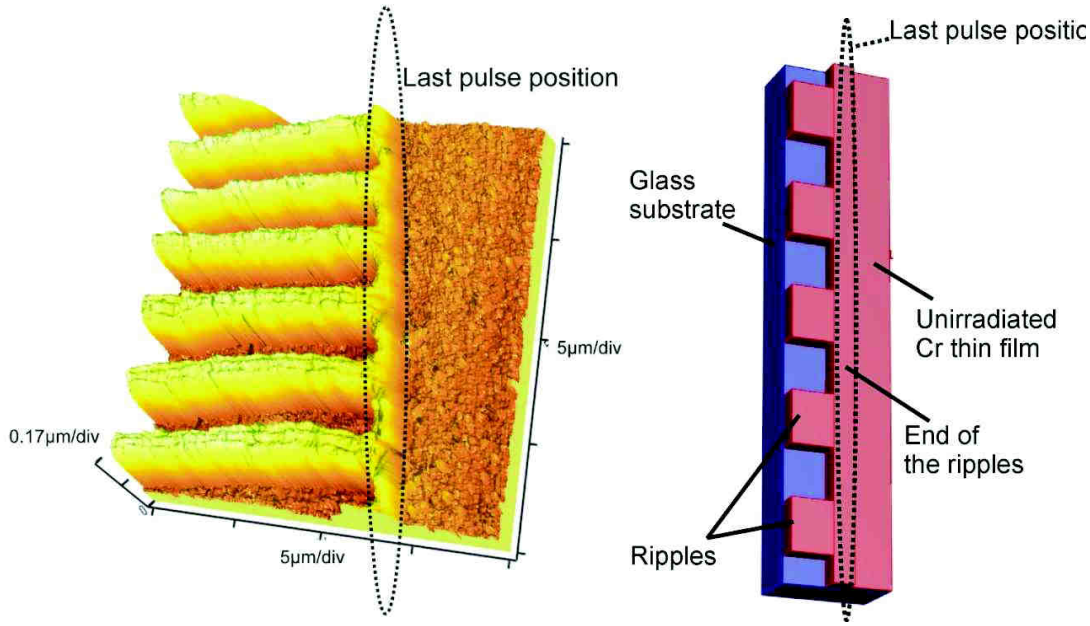

a) b)

Fig. 40 (a) The AFM image of the end of the ripples. Dot line represents location of an elliptical spot of the next laser pulse on the sample (the aspect ratio is not to scale). The thin chromium film is resolidified to periodical ripples on the left side of the image. On the right side of the image, there is the unmodified thin chromium film on the glass substrate. Laser fluence $F_0 = 1.9$ J·cm^{-2}, shift between pulses $\Delta x = 0.3$ μm, thickness of the thin chromium film $h = 100$ nm. (b) The geometry similar to the end of the ripples was used in simulation. Dot line represents an elliptical laser spot of the pulse on the sample (the aspect ratio is not to scale).

The simplified geometry (Fig. 40b) similar to the end of the ripple section (Fig. 40a) was designed in COMSOL Multiphysics to investigate the temperature field by numerically solving heat transfer Eq. (36). The aim of this modeling was to investigate the temperature distribution in thin metal film close to the end of ripples when the laser pulse heats the metal. The head source was simplified to a linear spot given by:

$$I(t) = \frac{F}{\tau_p} \mathrm{rect}\left(t/\tau_p\right), \tag{53}$$

where $F = F(x, y)$ is the laser fluence distribution in the pulse given by Eq. (50), laser beam has uniform intensity distribution in y direction because $w_{y0} >> y$ in the computational area and the Gaussian profile in x direction, the rectangular function denotes the step-like temporal profile of the laser pulse. The sample was heated in the position where the last laser pulse hit the sample (marked elliptical dot line in Fig. 40) in the back-side irradiation geometry, from the glass substrate. The incident laser fluence in the center of the beam was $F_0 = 1.0$ J·cm^{-2}, and the pulse duration $\tau_p = 10$ ns. The chromium and glass physical parameters were taken from Table 1 and Table 4, respectively. The calculated temperature distribution at the end of the laser pulse is shown in Fig. 41.

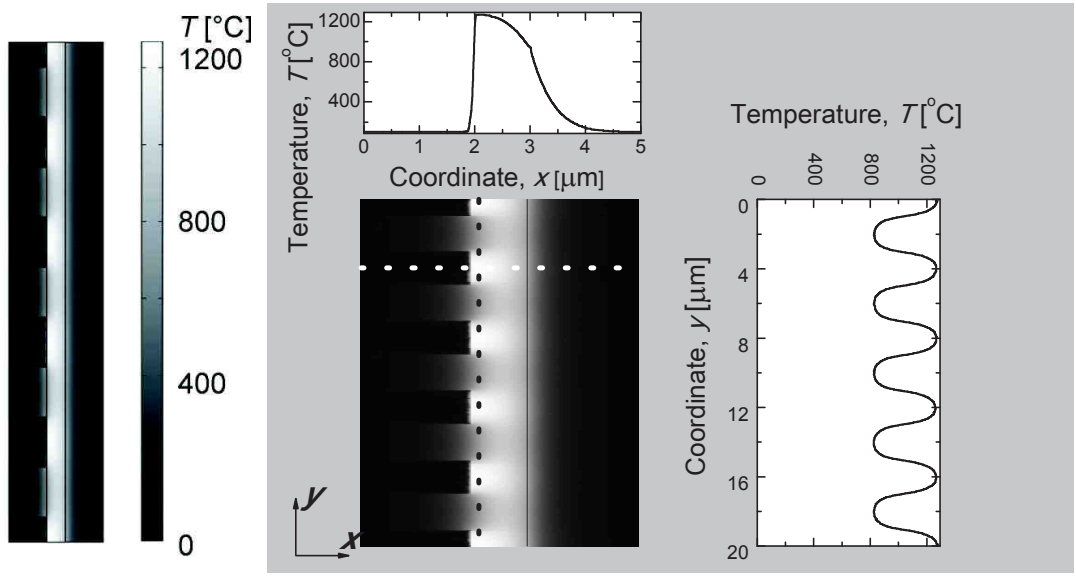

a) b)

Fig. 41 (a) The temperature distribution in the chromium film irradiated with a linear laser spot at the interface of longitudinal ripples (left) and untreated film (right). (b) Top graph shows a large temperature gradient in x direction. The left graph shows the temperature modulation in y direction even that the laser heating source was uniform in y direction.

We analyzed temperature distribution in the metal film and the glass substrate, when the laser pulse focused to a line was absorbed by the metal. Ripples are a

good heat sink for the absorbed laser energy. The temperature of chromium between ripples was at least 400 ºC higher than in areas where the ridge had contact with a ripple line. The difference in temperature was high enough to provoke the Marangoni effect which resulted in movement of molten metal from hot areas to colder ones adding the material to the ripple lines. The surface tension and viscosity of melted chromium depend on temperature therefore the temperature gradient initiated mass flow from the ridge into ripples. Moreover, the temperature gradient in x direction also shifted the whole ridge towards the untreated metal.

7.2.3 Marangoni convection velocity for liquid chromium

In order to estimate if the temperature gradient and time until metal remains molten is enough for redeployment of chromium from the ridge to ripples, manipulations with material and process parameters were performed.

Marangoni velocity can be evaluated by using Eq. (7). For this we theoretically computed the viscosity of the liquid Cr metal by using Eq. (46) $\eta_{\mathrm{m}} \approx 4.7\ \mathrm{mPa \cdot s}$, similar to the value which can be found in [148, 168]. For a liquid Cr at the melting point, the surface tension calculated by using Eq. (47) was γ_{m}=2100 $\mathrm{mN \cdot m^{-1}}$ while the exact measured value is γ_{m}=1780 $\mathrm{mN \cdot m^{-1}}$. Similar values of surface tension of liquid chromium can be found in [39, 164, 169, 170]. The temperature coefficient of the surface tension is $\partial\gamma/\partial T = -0.544\ \mathrm{mN \cdot m^{-1} \cdot K^{-1}}$, and similar values were measured for many liquid metals [40, 171, 172]. The temperature coefficients of surface tension can be estimated by using Eq. (49). The Marangoni speed estimated by using Eq. (7) is equal to $u = 10\ \mathrm{m \cdot s^{-1}}$. The same order of magnitude of the Marangoni speed of 60 $\mathrm{m \cdot s^{-1}}$ was found for gold nanobump formation on a glass substrate by Kuznetsov et al. [42] and the value of 80 $\mathrm{m \cdot s^{-1}}$ was found by Ivanov et al. [173].

The cooling rates obtained for the thin chromium film are $\sim 3\times10^{10}$ K·s^{-1} close to the solidification temperature and may be as high as $\sim 10^{11}$ K·s^{-1} during the liquid phase cooling [153].

The laser pulse heats chromium until it reaches the evaporating temperature T_v. Then the heat dissipates to the glass substrate due to diffusion, or to the surrounding air due to the convection and the black body radiation. Then the film reaches T_m. The time when chromium remains molten can be estimated by dividing $T_v - T_m$ by the cooling rate of the liquid phase and the value is of the order of 100 ns (the same time calculated for gold on quartz [135] and molybdenum on quartz [174] as well as for niobium including a phase transition.

Finally, the distance that molten chromium travels because of the Marangoni convection before it solidifies can be evaluated by multiplying the Marangoni speed and the time of the liquid phase existence: $10\,\mathrm{m\cdot s^{-1}} \times 100\,\mathrm{ns} = 1\,\mu\mathrm{m}$. The calculated value corresponds to a quarter of the ripple period in the thin chromium film. That means that the Marangoni convection under our experimental conditions is able to move molten metal from the ridge to ripples.

The Marangoni effect of moving free surface of liquid chromium was additionally simulated by using the finite element modeling software COMSOL Multiphysics. For this purpose, the full incompressible Navier-Stokes Eq. (10) and heat transfer Eq. (36) were solved two-dimensionally. The evolution of the end of the ripple structure heated with the laser pulse is given in Fig. 42.

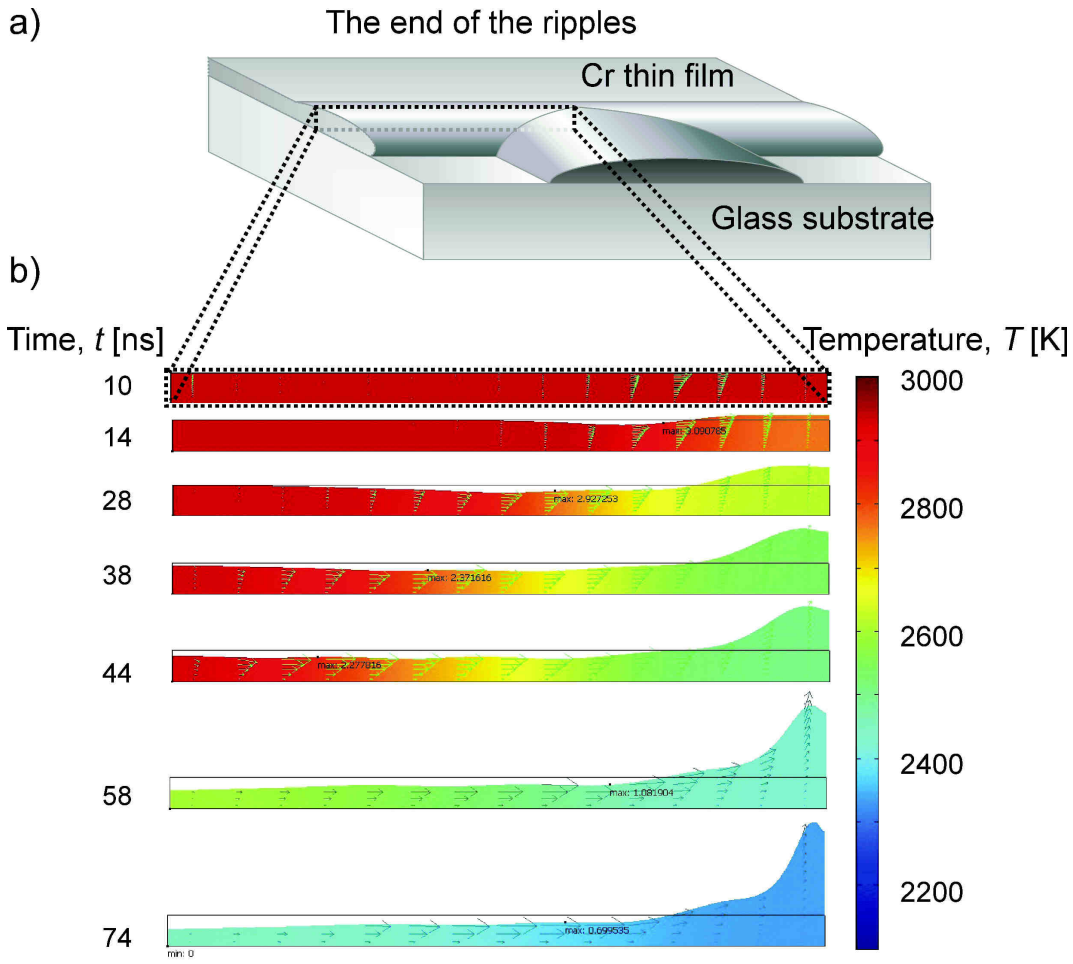

Fig. 42 Simulation of melt flow during the ripple growth. (a) scheme of the end of the ripple structure. (b) evolution of the thin chromium film in time after laser irradiation. Temperature is scaled in colors and velocity field is depicted in arrows. Molten metal in the ridge is pushed due to Marangoni (thermo-capillarity) forces from the area between the ripple lines to a location of the ridge-ripple interface.

Considering the fact that the only force active in the model was the surface tension dependence on temperature, we can state that the Marangoni effect plays a significant role in continuous formation of ripples in thin metal films.

7.3 CONCLUSIONS

Different physical phenomena were numerically tested if they could be responsible for the regular ripple formation in the thin chromium film on glass.

The model of ripple formation under irradiation with partially overlapping laser pulses was created which is in agreement with the experimental data and results of numerical simulation.

The Plateau-Rayleigh instability modulates the ridge of molten metal at the rim of the laser ablated area into droplets which are initial seeds for the regular ripple growth by redeployment of the molten metal due to Marangoni (thermo-capillarity) forces.

LIST OF CONCLUSIONS

1. Partially overlapping laser pulses initiated self-organization in the chromium thin film on glass when laser fluences exceeded the single pulse ablation (film removal) threshold. Formation of regular structures, ripples, took place in the 100 nm-thick chromium film when laser fluence was in the range of 1.7-2.7 $J \cdot cm^{-2}$ and a shift between pulses was in the range of 0.3-0.6 μm under our experimental conditions (focusing). The ripples were located periodically ($\Lambda \approx 4$ μm) parallel to the laser pulse shift direction.
2. The regular ripple structure stabilized after applying 3-5 partially overlapping laser pulses. If a defect was in the film, the regular structure was healed over again after applying another 3-5 laser pulses after the defect.
3. Periodical gratings of ripples with the unlimited length of lines can be manufactured in the metal film by the laser induced self-organization under irradiation with overlapping laser pulses.
4. The period of the grating made of regular ripples can be varied in the range from 2.5 to 4 μm. The period increases linearly by increasing the laser pulse fluence and decreases linearly by increasing the shift between pulses.
5. Diverse behavior of the metal films on glass was observed after irradiation with a sequence of partially overlapping laser pulses when the energy density was above the single-pulse ablation threshold. Regular longitudinal ripples were specific to the chromium film and also to the gold film in a very narrow window of the process parameters.
6. The model of ripple formation under irradiation with partially overlapping laser pulses which is in agreement with the experimental data and results of numerical simulation was created. The Plateau-Rayleigh instability modulates the ridge of molten metal at the rim of the laser-ablated area into droplets which are initial seeds for the regular ripple growth. The temperature modulation along the irradiation line is high enough to cause the Marangoni convection which results in movement of the molten metal from hot to colder areas.

SUMMARY

The present PhD thesis is the experimental and theoretical analysis of ripple formation in the thin chromium film on a glass substrate under irradiation with a sequence of partially overlapping laser pulses. The beam of a nanosecond laser tightly focused to a line was applied for the back-side ablation of the thin chromium film on the glass substrate. The stripe-like area ablated with a single laser pulse had cylindrical ridges of the melted metal. The partially overlapping pulses formed a complicated structure made of the metal remaining from the ridges. Regular structures, ripples, were formed when laser fluence was slightly above the single-pulse removal threshold and the shift between pulses was less than half width of the stripe ablated with a single laser pulse. The regular ripples were located periodically with the period of 2.5 – 4 μm. Ripples were orientated perpendicularly to the long axis of the beam spot and their length increased with every shifted pulse. Formation of regular diffraction gratings was experimentally implemented by using the above-mentioned technique. The grating period changed linearly with the laser fluence and it decreased with increasing the shift between pulses. Different models of the ripple formation in the thin metal film were considered, and the Plateau-Rayleigh instability of the cylindrical ridge formation during laser ablation appeared to be the most probable process responsible for initiation of the ripple formation. The Marangoni convection of the molten metal from hot areas to cold ones was the stabilizing process of the steady ripple formation. The possible ripple formation was investigated in different metal films on the glass substrate: aluminum, copper, gold and silve. Diverse behavior of the films depending on the metal, the shift between pulses and laser fluence was observed. Strong film adhesion to the glass substrate was important for ridge formation. The cylindrical ridge formation during laser ablation was found to be essential for initiation of the ripple formation.

REFERENCES

[1] D. F. Horne, Optical scales, reticles, gratings, masks, and standards. *Appl. Opt.* **20**, 4000-4008 (1981).

[2] C. Yang and Y. Shen, Laser direct writing system and its lithography properties. *Proc. SPIE* **3550**, 409 (1998).

[3] H. J. Levinson, *Principles of Lithography*. 3 edn (SPIE, Bellingham, 2010).

[4] Y. Sarov *et al.*, Fabrication of diffraction gratings for microfluidic analysis. *Bulg. J. Phys.* **29**, 17-29 (2002).

[5] A. Hirai, M. Kajima and S. Telada in *Handbook of Optical Metrology: Principles and Applications* (ed. T. Yoshizawa) Ch. 16, 393-410 (CRC Press, Boca Raton, 2008).

[6] S. Merino, A. Retolaza and I. Lizuain, Linear optical encoders manufactured by imprint lithography. *Microelectron. Eng.* **83**, 897-901 (2006).

[7] H. A. Macleod, *Thin-Film Optical Filters* (CRC Press, Boca Raton, 2010).

[8] H.-E. Schaefer, *Nanoscience: The Science of the Small in Physics, Engineering, Chemistry, Biology and Medicine* (Springer, Berlin, 2010).

[9] K. K. B. Hon, L. Li and I. M. Hutchings, Direct writing technology--Advances and developments. *CIRP Annals - Manufacturing Technol.* **57**, 601-620 (2008).

[10] J.-G. Kim, S.-H. Cho, T.-J. Je, D.-S. Choi and K.-H. Whang, Surface pattern formation on Cr thin film with ultrafast laser pulse. *Appl. Phys. A* **101**, 345-348 (2010).

[11] F. Mücklich and A. F. Lasagni in *Functional Properties of Bio-Inspired Surfaces* (eds E. A. Favret and N. O. Fuentes) Ch. 10, 281-308 (World Sci. Publishing Co., Singapore, 2009).

[12] K. Venkatakrishnan, P. Stanley, B. K. A. Ngoi, B. Tan and L. E. N. Lim, Femtosecond pulsed laser direct writing system. *Opt. Eng.* **41**, 1441-1445 (2002).

[13] Y. Morishige, High-accuracy laser mask repair technology using ps UV solid state laser. *Proc. SPIE* **4426**, 416-423 (2002).

[14] T. Okamoto, Y. Morishige, E. Ohmura, T. Sano and I. Miyamoto, Femtosecond laser ablation of Cr-SiO_2 binary mask. *Proc. SPIE* **4830**, 510-514 (2003).

[15] K. Regelskis and G. Račiukaitis. Method and equipment for grating formation. Lithuania patent (2006).

[16] O. Varlamova, F. Costache, J. Reif and M. Bestehorn, Self-organized pattern formation upon femtosecond laser ablation by circularly polarized light. *Appl. Surf. Sci.* **252**, 4702-4706 (2006).

[17] M. Birnbaum, Semiconductor Surface Damage Produced by Ruby Lasers. *J. Appl. Phys.* **36**, 3688-3689 (1965).

[18] J. E. Sipe, J. F. Young, J. S. Preston and H. M. Van Driel, Laser-induced periodic surface structure. I. Theory. *Phys. Rev. B* **27**, 1141-1154 (1983).
[19] D. C. Emmony, R. P. Howson and L. J. Willis, Laser mirror damage in germanium at 10.6 mu m. *Appl. Phys. Lett.* **23**, 598-600 (1973).
[20] J. F. Young, J. S. Preston, H. M. Van Driel and J. E. Sipe, Laser-induced periodic surface structure. II. Experiments on Ge, Si, Al, and brass. *Phys. Rev. B* **27**, 1155 (1983).
[21] P. M. Fauchet and A. E. Siegmann, Observation of higher-order laser-induced surface ripples on <111> germanium. *Appl. Phys. A* **32**, 135-140 (1983).
[22] Q.-Z. Zhao, S. Malzer and L.-J. Wang, Self-organized tungsten nanospikes grown on subwavelength ripples induced by femtosecond laser pulses. *Opt. Express* **15**, 15741-15746 (2007).
[23] M. Csete and Z. Bor, Laser-induced periodic surface structure formation on polyethylene-terephthalate. *Appl. Surf. Sci.* **133**, 5-16 (1998).
[24] X. C. Wang, G. C. Lim, F. L. Ng, W. Liu and S. J. Chua, Femtosecond pulsed laser-induced periodic surface structures on GaN/sapphire. *Appl. Surf. Sci.* **252**, 1492-1497 (2005).
[25] A. Borowiec and H. K. Haugen, Subwavelength ripple formation on the surfaces of compound semiconductors irradiated with femtosecond laser pulses. *Appl. Phys. Lett.* **82**, 4462-4464 (2003).
[26] M. Y. Shen *et al.*, Formation of regular arrays of silicon microspikes by femtosecond laser irradiation through a mask. *Appl. Phys. Lett.* **82**, 1715-1717 (2003).
[27] M. Schade *et al.*, High-resolution investigations of ripple structures formed by femtosecond laser irradiation of silicon. *Anal. Bioanal. Chem.* **396**, 1905-1911 (2010).
[28] J. Reif, F. Costache, M. Henyk and S. V. Pandelov, Ripples revisited: non-classical morphology at the bottom of femtosecond laser ablation craters in transparent dielectrics. *Appl. Surf. Sci.* **197-198**, 891-895 (2002).
[29] R. Böhme, C. Vass, B. Hopp and K. Zimmer, Sub-wavelength ripples in fused silica after irradiation of the solid/liquid interface with ultrashort laser pulses. *Nanotechnol.* **19**, 495301 (2008).
[30] J. Krüger *et al.*, Laser micromachining of barium aluminium borosilicate glass with pulse durations between 20 fs and 3 ps. *Appl. Surf. Sci.* **127-129**, 892-898 (1998).
[31] G. Daminelli, J. Krüger and W. Kautek, Femtosecond laser interaction with silicon under water confinement. *Thin Solid Films* **467**, 334-341 (2004).
[32] S. Baudach, J. Bonse and W. Kautek, Ablation experiments on polyamide with femtosecond laser pulses. *Appl. Phys. A* **69**, S395-S398 (1999).

[33] K. W. Kolasinski, Solid structure formation during the liquid/solid phase transition. *Current Opinion Solid State Mater. Sci.* **11**, 76-85 (2007).
[34] Q. Wu *et al.*, Femtosecond laser-induced periodic surface structure on diamond film. *Appl. Phys. Lett.* **82**, 1703-1705 (2003).
[35] P. Mogyorósi, K. Piglmayer and D. Bäuerle, Ar^+ laser-induced chemical etching of molybdenum in chlorine atmosphere. *Surf. Sci.* **208**, 232-244 (1989).
[36] P. B. Kargl, R. Kullmer and D. Bäuerle, Periodic structures in pyrolytic laser-CVD of W from WCl_6. *Appl. Phys. A* **57**, 175-179 (1993).
[37] R. L. Chapman, J. C. C. Fan, H. J. Zeiger and R. P. Gale, Crystallization-front velocity during scanned laser crystallization of amorphous Ge film. *Appl. Phys. Lett.* **37**, 292 (1980).
[38] G. Auvert *et al.*, Influence of cw laser scan speed in solid-phase crystallization of amorphous Si film on Si_3N_4/glass substrate. *Appl. Phys. Lett.* **38**, 613 - 615 (1981).
[39] B. C. Allen in *Liquid Metals, Chemistry and Physics* (ed. S. Z. Beer) 161-212 (Marcel Dekker, New York, 1972).
[40] I. Takamichi and R. I. L. Guthrie, *The physical properties of liquid metals* (Clarendon Press, Oxford, 1988).
[41] H.-J. Butt and M. Kappl, *Surface and Interfacial Forces* (Wiley, Weinheim, 2010).
[42] A. Kuznetsov, J. Koch and B. Chichkov, Nanostructuring of thin gold films by femtosecond lasers. *Appl. Phys. A* **94**, 221-230 (2009).
[43] J. Koch *et al.*, Nanotexturing of gold films by femtosecond laser-induced melt dynamics. *Appl. Phys. A* **81**, 325-328 (2005).
[44] K. Wissenbach *et al.* in *Tailored Light 2* (ed. R. Poprawe) 173-240 (Springer, Berlin, 2011).
[45] M. D'alessandria, A. Lasagni and F. Mücklich, Direct micro-patterning of aluminum substrates via laser interference metallurgy. *Appl. Surf. Sci.* **255**, 3210-3216 (2008).
[46] H. Ferziger and M. Peric, *Computational Methods for Fluid Dynamics* (Springer, Berlin, 2002).
[47] Y. Kaganovskii, H. Vladomirsky and M. Rosenbluh, Periodic lines and holes produced in thin Au films by pulsed laser irradiation. *J. Appl. Phys.* **100**, 044317 (2006).
[48] T. Schwarz-Selinger, D. G. Cahill, S. C. Chen, S. J. Moon and C. P. Grigoropoulos, Micron-scale modifications of Si surface morphology by pulsed-laser texturing. *Phys. Rev. B* **64**, 155323 (2001).
[49] A. Habenicht, M. Olapinski, F. Burmeister, P. Leiderer and J. Boneberg, Jumping Nanodroplets. *Science* **309**, 2043-2045 (2005).
[50] P. D. Rack, Y. Guan, J. D. Fowlkes, A. V. Melechko and M. L. Simpson, Pulsed laser dewetting of patterned thin metal films: A means of directed assembly. *Appl. Phys. Lett.* **92**, 223108-223103 (2008).

[51] A. Lasagni, M. D'alessandria, R. Giovanelli and F. Mücklich, Advanced design of periodical architectures in bulk metals by means of Laser Interference Metallurgy. *Appl. Surf. Sci.* **254**, 930-936 (2007).
[52] J. Svensson, N. M. Bulgakova, O. A. Nerushev and E. E. B. Campbell, Marangoni effect in SiO_2 during field-directed chemical vapor deposition growth of carbon nanotubes. *Phys. Rev. B* **73**, 205413 (2006).
[53] T. Debroy and S. A. David, Physical processes in fusion welding. *Rev. Mod. Phys.* **67**, 85 (1995).
[54] V. S. Ajaev and D. A. Willis, Thermocapillary flow and rupture in films of molten metal on a substrate. *Phys. Fluids* **15**, 3144-3150 (2003).
[55] D. A. Willis and X. Xu, Transport Phenomena and Droplet Formation During Pulsed Laser Interaction With Thin Films. *J. Heat Transfer* **122**, 763-770 (2000).
[56] T. E. Faber, *Fluid Dynamics for Physicists* (Cambridge, New York, 1995).
[57] D. Joseph, T. Funada and J. Wang, *Potential Flows of Viscous and Viscoelastic Liquids*. 1 edn (Cambridge, New York, 2008).
[58] V. Cardoso and Ó. J. C. Dias, Rayleigh-Plateau and Gregory-Laflamme Instabilities of Black Strings. *Phys. Rev. Lett.* **96**, 181601 (2006).
[59] A. Bid, A. Bora and A. K. Raychaudhuri, Experimental study of Rayleigh instability in metallic nanowires using resistance fluctuations measurements from 77K to 375K. *Proc. SPIE* **5843**, 147-154 (2005).
[60] A. Sharma and R. Khanna, Pattern Formation in Unstable Thin Liquid Films. *Phys. Rev. Lett.* **81**, 3463 (1998).
[61] C. Favazza, H. Krishna, R. Sureshkumar and R. Kalyanaraman, Nanomanufacturing via fast laser-induced self-organization in thin metal films. *Proc. SPIE* **6648**, 664809 (2007).
[62] A. Oron, S. H. Davis and S. G. Bankoff, Long-scale evolution of thin liquid films. *Rev. Mod. Phys.* **69**, 931 (1997).
[63] J. P. De Silva *et al.*, Switching Layer Stability in a Polymer Bilayer by Thickness Variation. *Phys. Rev. Lett.* **98**, 267802 (2007).
[64] J. Trice *et al.*, Novel Self-Organization Mechanism in Ultrathin Liquid Films: Theory and Experiment. *Phys. Rev. Lett.* **101**, 017802 (2008).
[65] A. M. Higgins and R. a. L. Jones, Anisotropic spinodal dewetting as a route to self-assembly of patterned surfaces. *Nature* **404**, 476-478 (2000).
[66] S. Herminghaus *et al.*, Spinodal Dewetting in Liquid Crystal and Liquid Metal Films. *Science* **282**, 916-919 (1998).
[67] J. A. Diez and L. Kondic, Computing Three-Dimensional Thin Film Flows Including Contact Lines. *J. Comput. Phys.* **183**, 274-306 (2002).
[68] J. A. Diez, L. Kondic and A. Bertozzi, Global models for moving contact lines. *Phys. Rev. E* **63**, 011208 (2000).
[69] R. Konnur, K. Kargupta and A. Sharma, Instability and Morphology of Thin Liquid Films on Chemically Heterogeneous Substrates. *Phys. Rev. Lett.* **84**, 931 (2000).

[70] A. V. Hershey, Ridges in a Liquid Surface Due to the Temperature Dependence of Surface Tension. *Phys. Rev.* **56**, 204 (1939).
[71] U. Thiele *et al.*, Modelling approaches to the dewetting of evaporating thin films of nanoparticle suspensions. *J. Phys.* **21**, 264016 (2009).
[72] V. Ajaev, J. Klentzman, C. Sodtke and P. Stephan, Mathematical modeling of moving contact lines in heat transfer applications. *Microgravity Sci. Technol.* **19**, 23-26 (2007).
[73] A. L. Bertozzi, The Mathematics of Moving Contact Lines in Thin Liquid Films. *Not. AMS* **45**, 689-697 (1998).
[74] J. Huang, A. R. Tao, S. Connor, R. He and P. Yang, A General Method for Assembling Single Colloidal Particle Lines. *Nano Lett.* **6**, 524-529 (2006).
[75] N. J. Suematsu, Y. Ogawa, Y. Yamamoto and T. Yamaguchi, Dewetting self-assembly of nanoparticles into hexagonal array of nanorings. *J. Colloid Interface Sci.* **310**, 648-652 (2007).
[76] P. G. Saffman and G. Taylor, The Penetration of a Fluid into a Porous Medium or Hele-Shaw Cell Containing a More Viscous Liquid. *Proc. Roy. Soc. A* **245**, 312-329 (1958).
[77] J. V. Maher, Development of Viscous Fingering Patterns. *Phys. Rev. Lett.* **54**, 1498-1501 (1985).
[78] A. M. Cazabat, F. Heslot, S. M. Troian and P. Carles, Fingering instability of thin spreading films driven by temperature gradients. *Nature* **346**, 824-826 (1990).
[79] A. V. Lyushnin, A. A. Golovin and L. M. Pismen, Fingering instability of thin evaporating liquid films. *Phys. Rev. E* **65**, 021602 (2002).
[80] A. A. Golovin, B. Y. Rubinstein and L. M. Pismen, Effect of van der Waals Interactions on the Fingering Instability of Thermally Driven Thin Wetting Films. *Langmuir* **17**, 3930-3936 (2001).
[81] J. B. Brzoska, F. Brochard-Wyart and F. Rondelez, Exponential Growth of Fingering Instabilities of Spreading Films Under Horizontal Thermal Gradients. *Europhys. Lett.* **19**, 97-102 (1992).
[82] I. Leizerson, S. G. Lipson and A. V. Lyushnin, Finger Instability in Wetting−Dewetting Phenomena. *Langmuir* **20**, 291-294 (2003).
[83] J. Sur, T. P. Witelski and R. P. Behringer, Steady-Profile Fingering Flows in Marangoni Driven Thin Films. *Phys. Rev. Lett.* **93**, 247803 (2004).
[84] D. E. Kataoka and S. M. Troian, A Theoretical Study of Instabilities at the Advancing Front of Thermally Driven Coating Films. *J. Coll. Interface Sci.* **192**, 350-362 (1997).
[85] A. M. Cazabat, F. Heslot, P. Carles and S. M. Troian, Hydrodynamic Fingering Instability of Driven Wetting Films. *Adv. Coll. Interface Sci.* **39**, 61-75 (1992).
[86] H.-H. Yu and J. W. Hutchinson, Influence of substrate compliance on buckling delamination of thin films. *Int. J. Fracture* **113**, 39-55 (2002).
[87] P. Howell, G. Kozyreff and J. Ockendon, *Applied Solid Mechanics*, Vol. 43 (Cambridge, New York, 2009).

[88] C. M. Wang, J. N. Reddy and K. H. Lee, *Shear Deformable Beams and Plates* (Elsevier, Oxford, 2000).
[89] J. W. Dundurs, Edge-bonded dissimilar orthogonal elastic wedges. *J. Appl. Mech.* **36**, 650-652 (1969).
[90] A. A. Abdallah *et al.*, Buckle morphology of compressed inorganic thin layers on a polymer substrate. *Thin Solid Films* **503**, 167-176 (2006).
[91] A. A. Abdallah, P. C. P. Bouten, J. M. J. Den Toonder and G. De With, The effect of moisture on buckle delamination of thin inorganic layers on a polymer substrate. *Thin Solid Films* **516**, 1063-1073 (2008).
[92] C. Kittel, *Introduction to solid state physics*. 7 edn (Wiley, Toronto, 1996).
[93] T. Ye, Z. Suo and A. G. Evans, Thin film cracking and the roles of substrate and interface. *Int. J. Solids Structures* **29**, 2639-2648 (1992).
[94] J. W. Hutchinson and Z. Suo in *Advances in Applied Mechanics* Vol. 29 (eds W. H. John and Y. W. Theodore) 63-191 (Elsevier, New York, 1991).
[95] S. Doyle *et al.*, Residual stress in Ni-Mn-Ga thin films deposited on different substrates. *Eur. Phys. J. Spec. Top.* **158**, 99-105 (2008).
[96] Y. P. Meshcheryakov and N. M. Bulgakova, Thermoelastic modeling of microbump and nanojet formation on nanosize gold films under femtosecond laser irradiation. *Appl. Phys. A* **82**, 363-368 (2006).
[97] O. S. Heavens, Optical properties of thin films. *Rep. Prog. Phys.* **23**, 1 (1960).
[98] V. P. Veiko, *Laser Processing of Film Components* (Mashinostroenie, Leningrad, 1986).
[99] J. Siegel, E. Matthias, K. Ettrich and E. Welsch, UV-laser ablation of ductile and brittle metal films. *Appl. Phys. A* **64**, 213-218 (1997).
[100] D. C. Agrawal and R. Raj, Measurement of the ultimate shear strength of a metal-ceramic interface. *Acta Metall.* **37**, 1265-1270 (1989).
[101] B. F. Chen, J. Hwang, I. F. Chen, G. P. Yu and J. H. Huang, A tensile-film-cracking model for evaluating interfacial shear strength of elastic film on ductile substrate. *Surf. Coatings Technol.* **126**, 91-95 (2000).
[102] C. Xie and W. Tong, Cracking and decohesion of a thin Al_2O_3 film on a ductile Al-5%Mg substrate. *Acta Materialia* **53**, 477-485 (2005).
[103] W.-J. Chou, G.-P. Yu and J.-H. Huang, Mechanical properties of TiN thin film coatings on 304 stainless steel substrates. *Surf. Coatings Technol.* **149**, 7-13 (2002).
[104] M. Cordill, A. Taylor, J. Schalko and G. Dehm, Fracture and Delamination of Chromium Thin Films on Polymer Substrates. *Metall. Mater. Trans. A* **41**, 870-875 (2010).
[105] B. B. Guzina, D. H. Timm and V. R. Voller, Crack spacing in strained films. *J. Phys. IV France* **120**, 201-208 (2004).
[106] O. Stenzel in *The Physics of Thin Film Optical Spectra* (eds G. Ertl, H. Luth and D. L. Mills) Ch. 6, 71-100 (Springer, Berlin, 2005).
[107] M. Fox, *Optical Properties of Solids* (Oxford, New York, 2001).

[108] R. Wester in *Tailored Light 2* (ed. R. Poprawe) 43-62 (Springer, Berlin, 2011).
[109] I. N. Mihailescu and J. Hermann in *Laser Processing of Materials* (ed. P. Schaaf) Ch. 4, 49-88 (Springer, Berlin, 2010).
[110] A. Kruusing, *Handbook of Liquids-Assisted Laser Processing* (Elsevier, Oxford, 2008).
[111] N. M. Bulgakova, A. V. Bulgakov and L. P. Babich, Energy balance of pulsed laser ablation: thermal model revised. *Appl. Phys. A* **79**, 1323-1326 (2004).
[112] J. Bovatsek, A. Tamhankar, R. S. Patel, N. M. Bulgakova and J. Bonse, Thin film removal mechanisms in ns-laser processing of photovoltaic materials. *Thin Solid Films* **518**, 2897-2904 (2010).
[113] N. M. Bulgakova and A. V. Bulgakov, Pulsed laser ablation of solids: transition from normal vaporization to phase explosion. *Appl. Phys. A* **73**, 199-208 (2001).
[114] L. Jiang and H.-L. Tsai, Improved Two-Temperature Model and Its Application in Ultrashort Laser Heating of Metal Films. *J. Heat Transfer* **127**, 1167-1173 (2005).
[115] Y. Zhang and J. K. Chen, Ultrafast melting and resolidification of gold particle irradiated by pico- to femtosecond lasers. *J. Appl. Phys.* **104**, 054910-054919 (2008).
[116] S. I. Anisimov, B. L. Kapeliovich and T. L. Perelman, Electron emission from metal surfaces exposed to ultrashort laser pulses. *Sov. Phys. JETP* **39**, 375-377 (1974).
[117] J. K. Chen, D. Y. Tzou and J. E. Beraun, A semiclassical two-temperature model for ultrafast laser heating. *Int. J. Heat Mass Transfer* **49**, 307-316 (2006).
[118] B. H. Christensen, K. Vestentoft and P. Balling, Short-pulse ablation rates and the two-temperature model. *Appl. Surf. Sci.* **253**, 6347-6352 (2007).
[119] H. Hirori, T. Tachizaki, O. Matsuda and O. B. Wright, Electron dynamics in chromium probed with 20-fs optical pulses. *Phys. Rev. B* **68**, 113102 (2003).
[120] S. D. Brorson *et al.*, Femtosecond room-temperature measurement of the electron-phonon coupling constant gamma in metallic superconductors. *Phys. Rev. Lett.* **64**, 2172 (1990).
[121] L. V. Zhigilei *et al.* in *Laser-Surface Interactions for New Materials Production – Tailoring Structure* (eds A. Miotello and P. M. Ossi) 43-72 (Springer, New York, 2010).
[122] M. Beresna, T. Gertus, R. Tomašiūnas, H. Misawa and S. Juodkazis, Three-Dimensional Modeling of the Heat-Affected Zone in Laser Machining Applications. *Hindawi Publishing Corporation Laser Chem.* **976205**, 1-6 (2008).
[123] J. M. Liu, Simple technique for measurements of pulsed Gaussian-beam spot sizes. *Opt. Lett.* **7**, 196-198 (1982).

[124] J. Bonse, J. M. Wrobel, J. Krüger and W. Kautek, Ultrashort-pulse laser ablation of indium phosphide in air. *Appl. Phys. A* **72**, 89-94 (2001).
[125] D. Klinger *et al.*, Surface modification of polymethylmethacrylate irradiated with 60 fs single laser pulses. *Radiat. Phys. Chem.* **78**, S71-S74 (2009).
[126] *Fundamentals of Photonics* (ed. B. E. A. Saleh and M. C. Teich) (John Wiley & Sons, New York, 1991).
[127] R. Srinivasan and B. Braren, Ablative photodecomposition of polymer films by pulsed far-ultraviolet (193 nm) laser radiation: Dependence of etch depth on experimental conditions. *J. Polym. Sci.* **22**, 2601-2609 (1984).
[128] J. E. Andrew, P. E. Dyer, D. Forster and P. H. Key, Direct etching of polymeric materials using a XeCl laser. *Appl. Phys. Lett.* **43**, 717-719 (1983).
[129] S. Nolte *et al.*, Ablation of metals by ultrashort laser pulses. *J. Opt. Soc. Am. B* **14**, 2716-2722 (1997).
[130] S. K. Lee, K. K. Yoon, K. H. Whang and S. J. Na, Excimer laser ablation removal of thin chromium films from glass substrates. *Surf. Coat. Technol.* **113**, 63-74 (1999).
[131] E. Ohmura, T. Okamoto, S. Fujiwara, T. Sano and I. Miyamoto, Chromium thin film ablation with double pulses of femtosecond laser. *J. Jpn. Soc. Precision Eng.* **71**, 284-289 (2005).
[132] Z. Han, C. Zhou, E. Dai and J. Xie, Ultrafast double pulses ablation of Cr film on glass. *Opt. Commun.* **281**, 4723-4726 (2008).
[133] W. Wang *et al.*, Damage mechanism and morphology characteristics of chromium film in femtosecond laser rear-side ablation. *Appl. Surf. Sci.* **256**, 3612-3617 (2010).
[134] J. Kim, S. Na, S. Cho, W. Chang and K. Whang, Surface ripple changes during Cr film ablation with a double ultrashort laser pulse. *Opt. Lasers Eng.* **46**, 306-310 (2008).
[135] X. Zhang, S. S. Chu, J. R. Ho and C. P. Grigoropoulos, Excimer laser ablation of thin gold films on a quartz crystal microbalance at various argon background pressures. *Appl. Phys. A* **64**, 545-552 (1997).
[136] Q. Xia, P. F. Murphy, H. Gao and S. Y. Chou, Ultrafast and selective reduction of sidewall roughness in silicon waveguides using self-perfection by liquefaction. *Nanotechnol.* **20**, 345302 (2009).
[137] K. Venkatakrishnan, B. Tan and B. K. A. Ngoi, Femtosecond pulsed laser ablation of thin gold film. *Opt. Laser Technol.* **34**, 199-202 (2002).
[138] S. Kopac, J. Pirs and J. Mozina, Optodynamic analysis of direct laser writing of graduation lines. *Appl. Phys. A* **62**, 77-82 (1995).
[139] A. Misra, S. Fayeulle, H. Kung, T. E. Mitchell and M. Nastasi, Residual stresses and ion implantation effects in Cr thin films. *Nucl. Instrum. Methods Phys. Res. Sec. B* **148**, 211-215 (1999).
[140] G. C. J. Rouweler, Van der Waals forces between fused silica and fused silica covered with a chromium layer. *Chem. Phys. Lett.* **8**, 275-276 (1971).

[141] *American Institute of Physics Handbook*. 3 edn (ed. D. E. Gray) (McGraw-Hill, New York, 1972).
[142] W. E. Motzer in *Chromium (VI) Handbook* (eds J. Guertin, J. A. Jacobs and C. P. Avakian) 23-92 (CRC, Boca Raton, 2005).
[143] A. Goldsmith, T. E. Waterman and H. J. Hirschhorn, *Handbook of Thermophysical Properties of Solid Materials*, Vol. I (Macmillan, New York, 1961).
[144] N. W. Ashcroft and N. D. Mermin, *Solid State Physics* (Harcourt, USA, 1976).
[145] P. B. Johnson and R. W. Christy, Optical constants of transition metals: Ti, V, Cr, Mn, Fe, Co, Ni, and Pd. *Phys. Rev. B* **9**, 5056 (1974).
[146] *Thermal Expansion of Solids* Vol. 1-4 (ed. R. E. Taylor) (ASM International, USA, 1998).
[147] W. B. Chung, K. Nogi, W. A. Miller and A. Mclean, Surface Tension of Liquid Cr-O System. *Mater. Trans. JIM* **33**, 753-757 (1992).
[148] G. Kaptay, A unified equation for the viscosity of pure liquid metals. *Z. Metallkd.* **96**, 1-8 (2005).
[149] J. Kim and S. Na, Metal thin film ablation with femtosecond pulsed laser. *Opt. Laser Technol.* **39**, 1443-1448 (2007).
[150] H. Gercek, Poisson's ratio values for rocks. *Int. J. Rock Mech. Min. Sci.* **44**, 1-13 (2007).
[151] Y. Matsumoto, S. Ohta, N. Aoki and M. Morinaga, Microscopic fracture mechanism of sintered high purity chromium. *Mater. Sci. Eng. A* **285**, 213-223 (2000).
[152] E. Matthias *et al.*, In-situ investigation of laser ablation of thin films. *Thin Solid Films* **254**, 139-146 (1995).
[153] A. Jain, V. Kulkarni and D. Sood, Pulsed laser heating calculations incorporating vapourization. *Appl. Phys. A* **25**, 127-133 (1981).
[154] E. Matthias *et al.*, The influence of thermal diffusion on laser ablation of metal films. *Appl. Phys. A* **58**, 129-136 (1994).
[155] R. Novakovic, E. Ricci, D. Giuranno and A. Passerone, Surface and transport properties of Ag-Cu liquid alloys. *Surf. Sci.* **576**, 175-187 (2005).
[156] K. J. Lee, J. W. Kang, P. S. Jeon, H. J. Kim and J. Yoo, The measurements of thermal diffusivity dependent on temperature for pure metals by the new photothermal displacement configuration. *Thermochimica Acta* **455**, 60-65 (2007).
[157] P. Benjamin and C. Weaver, The Adhesion of Evaporated Metal Films on Glass. *Proc. R. Soc. London, Ser. A* **261**, 516-531 (1961).
[158] I. Egry, E. Ricci, R. Novakovic and S. Ozawa, Surface tension of liquid metals and alloys - Recent developments. *Adv. Colloid Interface Sci.* **159**, 198-212 (2010).
[159] J. A. Balderas-Lopez and A. Mandelis, Thermal diffusivity measurements in the photoacoustic open-cell configuration using simple signal normalization techniques. *J. Appl. Phys.* **90**, 2273-2279 (2001).

[160] R. Novakovic, E. Ricci and F. Gnecco, Surface and transport properties of Au-In liquid alloys. *Surf. Sci.* **600**, 5051-5061 (2006).
[161] S. Choi, D. Kim and S.-H. Choa, Thermal Diffusivity of Metallic Thin Films: Au, Sn, Mo, and Al/Ti Alloy. *Int. J. Thermophys.* **27**, 1551-1563 (2006).
[162] U. Holzwarth and H. Stamm, Mechanical and thermomechanical properties of commercially pure chromium and chromium alloys. *J. Nucl. Mater.* **300**, 161-177 (2002).
[163] E. N. D. C. Andrade and E. R. Dobbs, The Viscosities of Liquid Lithium, Rubidium and Caesium. *Proc. R. Soc. London, Ser. A* **211**, 12-30 (1952).
[164] B. C. Allen, The Surface tension of liquid transition metals at their melting points. *Trans. AIME* **227**, 1175-1183 (1963).
[165] M. Elbandrawy and M. C. Gupta, Optical characteristics of femtosecond laser micromachined periodic structures in Si <100>. *Appl. Opt.* **45**, 7137-7143 (2006).
[166] A. S. Marathay in *Handbook of Optics* Vol. I (ed. M. Bass) Ch. 3, 3.1-3.31 (McGraw Hill, New York, 1995).
[167] B. Q. Yang and P. Li, Fracture Behavior of a Brittle Coating on an Elastic Substrate under Residual Stress. *Advanced Mater. Res.* **595**, 217-218 (2011).
[168] S. Lugomer, Z. Geretovszky and T. Szorenyi, Laser generation of regular wavy patterns by nonlinear instability of a metal nanolayer. *J. Appl. Phys.* **104**, 054911-054917 (2008).
[169] G. G. Stoney, The Tension of Metallic Films Deposited by Electrolysis. *Proc. R. Soc. Lond. A* **82**, 172-175 (1909).
[170] F. Xiao *et al.*, Surface tension of molten Ni-(Cr, Co, W) alloys and segregation of elements. *Trans. Nonferrous Met. Soc. China* **18**, 1184-1188 (2008).
[171] D. A. Harrison, D. Yan and S. Blairs, The surface tension of liquid copper. *J. Chem. Thermodyn.* **9**, 1111-1119 (1977).
[172] I. Egry, G. Lohoefer and G. Jacobs, Surface Tension of Liquid Metals: Results from Measurements on Ground and in Space. *Phys. Rev. Lett.* **75**, 4043 (1995).
[173] D. S. Ivanov *et al.*, Nanocrystalline structure of nanobump generated by localized photoexcitation of metal film. *J. Appl. Phys.* **107**, 013519-013517 (2010).
[174] J. Hermann *et al.*, Comparative investigation of solar cell thin film processing using nanosecond and femtosecond lasers. *J. Phys. D* **39**, 453 (2006).